Validated force-based modeling of pedestrian dynamics

Inaugural - Dissertation

zur

Erlangung des Doktorgrades

der Mathematisch-Naturwissenschaftlichen Fakultät

der Universität zu Köln

vorgelegt von

Mohcine Chraibi

aus Casablanca (Marokko)

Berichterstatter: Prof. Dr. Andreas Schadschneider

Prof. Dr. Armin Seyfried

Tag der mündlichen Prüfung: 15.05.2012

To my beloved son, Idris Tengis

ACKNOWLEDGEMENTS

Many thanks to all of the people who made this dissertation possible, especially Prof. Dr. Armin Seyfried, to whom I owe a deep debt of gratitude. From him I learned to become more rational, to recognize and avoid imprecise reasoning, especially in addressing problems and evaluating solutions.

Completing this dissertation would never have been possible without the enthusiastic supervision and guidance of Prof. Dr. Andreas Schadschneider. He was always ready for a fruitful and constructive discussion, especially when the topic was *force-based* models. Thanks to their "physical" sense, I learned to shun superficial and premature judgments of the type "it is obvious".

I also extend my thanks to all my colleagues at the *Jülich Supercomputing Centre*, in particular: Dr. Bernard Steffen for his valuable mathematical input; Mike Boltes for developing PeTrack, which made high precision trajectory-extraction possible; Ulrich Kemloh for creating TraVisTo – a tool that helped me visualize my countless bugs; and Stefan Holl for practicing French with me, correcting my texts and giving advice when I needed it most.

I shall be forever indebted to my parents, and my sisters, Salma, Hinda and Ghita, for their unshakable faith and absolute support, especially when all else failed and their backing was the only possible remedy.

Finally, I would like to thank my lovely wife, Ariunaa, for her companionship and untiring, unwavering support. She (somehow) managed to live for so many years with a chaotic student. Please do not stop doing so.

TABLE OF CONTENTS

LIST OF FIGURES

Figure

LIST OF APPENDICES

Appendix

LIST OF ABBREVIATIONS

CA Cellular Automata

CDT Collision Detection Technique

CFM Centrifugal Force Model

DCA Distance of Closest Approach

FD Fundamental Diagram

GCFM Generalized Centrifugal Force Model

ODE Ordinary Differential Equations

SFM Social Force Model

ABSTRACT

Force-based modeling of pedestrian dynamics: Assets and shortcomings

by

Mohcine Chraibi

This dissertation investigates force-based modeling of pedestrian dynamics. Having the quantitative validation of mathematical models in focus principle questions will be addressed throughout this work: Is it manageable to describe pedestrian dynamics solely with the equations of motion derived from the Newtonian dynamics? On the road to giving answers to this question we investigate the consequences and side-effects of completing a force-based model with additional rules and imposing restrictions on the state variables. Another important issue is the representation of modeled pedestrians. Does the geometrical shape of a two dimensional projection of the human body matter when modeling pedestrian movement? If yes which form is most suitable? This point is investigated in the second part while introducing a new force-based model. Moreover, we highlight a frequently underestimated aspect in force-based modeling which is to what extent the steering of pedestrians influences their dynamics? In the third part we introduce four possible strategies to define the desired direction of each pedestrian when moving in a facility.

Finally, the effects of the aforementioned approaches are discussed by means of numerical tests in different geometries with *one* set of model parameters. Furthermore, the validation of the developed model is questioned by comparing simulation results with empirical data.

KURZZUSAMMENFASSUNG

Kraftbasierte Modellierung der Fußgängerdynamik: Umfassende Evaluierung

von

Mohcine Chraibi

Diese Dissertation befasst sich mit der kraftbasierten Modellierung in der Fußgänger-dynamik. Mit Fokus auf die quantitative Validierung von mathematischen Modellen werden grundlegende Fragen untersucht. Ist es realistisch, mit den Bewegungsgleichungen der Newtonschen Dynamik die Fußgängerdynamik ausreichend gut zu beschreiben? Um diese Frage zu beantworten wird untersucht, welche Folgen und Nebenwirkungen zusätzliche Regeln sowie Beschränkungen der Zustandsvariablen für Kraftbasierte Modelle haben. Eine weitere wichtige Frage ist die Darstellung der modellierten Fußgänger. Welcher Einfluss hat die geometrische Form der zweidimensionalen Projektion des menschlichen Körpers auf die Modellierung der Fußgängerbewegung? Welche Form eignet sich am besten für diesen Zweck? Diese Fragen werden im zweiten Teil dieser Arbeit anhand eines neuen kraftbasierten Modells untersucht. Darüber hinaus befasst sich die Arbeit mit einem oft unterschätzten Aspekt der Kraftbasierten Modellierung. Welche Rolle spielt die Richtungssteuerung der Fußgänger auf die Dynamik des gesamten Systems? Im dritten Teil werden vier mögliche Strategien eingeführt, um die gewünschte Richtung jedes Fußgängers während einer Simulation zu definieren. Schließlich werden die Auswirkungen und Ergebnisse der oben genannten Ansätze mit Hilfe von numerischen Tests in verschiedenen Geometrien mit *einem* Satz von Modellparametern untersucht. Die Prüfung und Kalibrierung des entwickelten Modells auf Basis von empirischen Daten führt zu einer realistischen Einschätzung seiner Qualität.

RÉSUMÉ

Modélisation de la dynamique des piétons basée sur des forces: Avantages et lacunes

par

Mohcine Chraibi

Les modèles basés sur des forces sont une approche très populaire pour la modélisation de la dynamique des piétons. Cette approche suppose que le mouvement des piétons résulte de forces extérieures. Après avoir donné un aperçu sur l'état de l'art de la modélisation de la dynamique des piétons basée sur les forces, nous discutons les conséquences de compléter ces modèles avec des règles supplémentaires et des restrictions sur les variables d'état. Par ailleurs, la forme des piétons modélisés est étudiée. Il est suggéré que, dans un espace deux dimensionnel, une ellipse à axes dépendants de la vitesse décrit plus précisément le mouvement des piétons. La question concernant la façon de diriger les piétons vers un goulot (ou un virage) a été négligée au profit des forces de répulsion. À première vue, cela semble être compréhensible étant donné que les interactions entre les piétons en particulier dans les situations de haute densité dominent la dynamique globale de la foule. Toutefois, attribuer aux piétons une direction inappropriée pourrait avoir un impact négatif sur le résultat de la dynamique. À cet effet, une nouvelle méthode sera introduite afin de diriger les piétons et ainsi faciliter leur circulation en particulier dans les virages et dans les goulots. D'autres algorithmes ont été également étudiés. Ces trois aspects seront examinés au sein d'un nouveau modèl basé sur le principe des forces Vérification et étalonnage du modèl basée sur des donnés empiriques permettra une évaluation réaliste de sa qualité de décrire convenablement la dynamique des piétons.

مُلَخَّص

دِرَاسَةٌ مُعَمَّقَة لِنَمذجة دِينَامِيةِ المُشَاة عَلَى أَسَاسِ مَبدَإِ القِوَى

مِن

محسِّن شرَايِبي

مِن بَينِ أَهَمِ النَمُوذَجِيَات أَلَّتِي تَعني بِدِرَاسةِ دِينَامِيةِ المُشَاة، نَجِدُ النَمُوذَجِيَات المَبنِيَةُ عَلَى نَظَرِيةِ القِوَى. هَذَ النَوعُ مِنَ النَمُوذَجِيَات يَقُومُ عَلَى أَسَاسٍ إِفتِرَاضِية أَنَ حَرَكِيَةَ المُشَاةِ مَا هِيَ إِلَّا نِتَاجٌ عَن قِوَى خَارِجِيةٍ تُطَبَّقُ عَلَى المُشَاةِ و بِالتَّالِي تُحَدِّدُ مَسَارَاتِهِم. بَعدَ تَقدِيمٍ مُلَخَّصٍ قَصِيرٍ يَتِمُ فِيهِ تَقدِيمُ و شَرحُ أَحدَثِ النَمُوذَجِيَات، سَيَتِمُ التَطَرُّقُ لِدِرَاسةِ آثَارِ بَعضِ التِقنِيَاتِ الإِضَافِيةِ و الرَّامِيةُ إِلَى تَجَنُّبِ و حَلِّ المَشَاكِلِ الجَوهَرِيةِ الخَاصَةِ بِمَبدَإِ القِوَى. بَعدَ ذَالِكَ سَتَتِمُ دِرَاسةُ الشَّكلِ الهَندَسِي الأَكثَرُ صَلَاحِيةً لِتَمثِيلِ الجِسمِ البَشَرِي. وَنَتِيجَة لِذَالِكَ تَمَ التَّوَصُل إِلَى أَنَّ الشَّكلَ الإِهلِيلِجِي يُقَرِّبُ بِطَرِيقَةٍ أَكثَرَ دِقَةٍ الجِسمِ البَشَرِي فِي بُعدِهِ الثَّانِي. إِضَافَةً الَى ذَالِكَ سَوف يَتِمُ التَطَرُّقُ إِلَى كَيفِيةِ تَوجِيه المُشَاةِ بِنَاءً عَلَى تَحدِيدِ الإِتِّجَاهِ الصَّحِيح لِمُوَجِّهِ السُّرعَةِ المُرَادَةِ. سَنُبَيِّنُ انَ إِختِيَارًا صَائِبًا لِمُوَجِّهِ السُّرعَةِ المُرَادَةِ و بِالتَّالِي التَّحَكُمُ فِي القِوَى الدَافِعَة، هُوَ أَمرُ جِدَّ مُؤَثِّر عَلَى الدِينَامِيةِ العَامَّة و يَجِبُ التَّعَامُلُ مَعَهُ بِعنَايةٍ فَائِقَة. هَذِهِ الرَكَائِزِ الثَلَاثِ سَيَتِمُ بَلوَرَتُهَا فِي إِطَارِ نَمُوذَجٍ جَدِيدٍ لِمُعَايَرَةِ هَذَ النَمُوذَج و التَّحَقُّق مِن صِحَّتِهِ، سَيَتِّمُ اللُّجُوءُ إِلَى مُعطَيَاتٍ تَجرِيبِيَة إِسُتنِبطَت مِن تَجَارِبٍ تَمَ إِنجَازُهَا فِي ظُرُوفٍ مُختَبَرِيَّة.

CHAPTER I

Introduction

1.1 Mathematical modeling of pedestrian dynamics

Mathematical modeling is the attempt to describe, explain and learn about real-word phenomena by means of concepts. How to model a highway traffic or a crowd of football fans? Probably, there is no unique and rigorous answer to this kind of question. Certainly, to model those systems one should make some assumptions and "simplifications" to restrain the complexity of the system.

Obviously, a given phenomena can be represented by more than one model. This raises the question of criteria a model has to satisfy in order to be qualified as good or worthless. Essentially, it is difficult to quantify the quality of a given model in a rigorous manner. In other words the set of mathematical models is not ordered with respect to the relation "model $\mathcal{X}$ is better that model $\mathcal{Y}$". As a consequence there exists no "best model". Nevertheless, one can introduce criteria to characterize the quality of models, e.g. the formalization of Occam's razor: The minimum description length principle [92]. Thus statements like "model $\mathcal{X}$ is better that model $\mathcal{Y}$" makes only sense with respect to a certain principle or criterion.

This issue is not different in the study of pedestrians dynamics, where several models have been developed in the past. One can briefly define pedestrian dynamics as the study of properties and characteristics emerging from the collective motion

of pedestrians. In everyday life a pedestrian moves in space freely without any restrictions from his environment. However, up the time where a pedestrian enters a building or an area where in the same time other pedestrians reside, this "freedom" of movement becomes manifestly restricted. For the sake of example one thinks of the movement of individual pilgrims in crowds performing the *Tawaf* [12], where many thousand of people perform a nearly circular movement.

From a mathematical point of view, pedestrian dynamics is widely considered as an example of a complex system. In fact, a crowd can be interpreted as a complex system emerging from non-linear interacting individuals. This categorization seems to be comprehensible since a crowd is made up of a large number of individuals that interact in a non-trivial manner. This becomes even more clear if the following definition of a complex system is recalled:

"A system can be regarded as complex if it can be analyzed into many components having relatively many relations among them, so that the behavior of each component depends on the behavior of others" [109].

In order to predict the evolution of the crowd in cases where the movement of one pedestrian depends on the movement of others, several models and experiments were developed. Most of the models are based on physical analogies, i.e. fluids, particles, that could hardly be expected to exactly reproduce the dynamics of pedestrians. This is expectable, since on one hand a crowd is composed of heterogeneous and intelligent individuals and on the other hand the physical analogy is based on observations of qualitative properties of a crowd. Those observations can be significant or superficial.

In the past several aspects of pedestrian dynamics were investigated e.g., analysis of design issues of facilities in urban areas [58, 67], evacuation planning [118, 99, 114, 39, 93], computer animation [107, 119, 78] and computer vision [120, 98]. For further information we refer to the reviews [95, 96].

Independently of the investigated issue the central concern is how accurate and
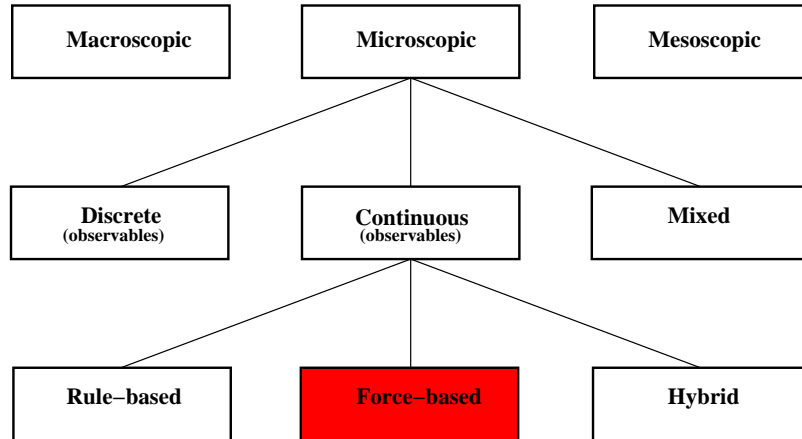
Figure 1.1: A possible hierarchical organization of models for pedestrian dynamics.

realistic the modeling of pedestrian dynamics is. For this purpose several mathematical models have been developed. In the next section a brief overview of existing models and their classification is given (see Fig. 1.1). This non-exclusive classification is based on some common properties that emerge from each model and is may not unique. It is a result of the author's attempt to analyze properties of the most elaborated and most used models. For a more detailed overview the reader may refer to [94].

1.2 Macroscopic models

Macroscopic models describe the state of a system with aggregate observables e.g. of density and flow. The state of individuals is not in the center of the macroscopic interpretation but rather the dynamics in the aggregate of the whole crowd.

In large-scale events, e.g. *Hajj*, Love Parade and music concerts, regions of high density occur and could remain over a relatively long time period. In such cases the degree of freedom of each individual is limited, thus an analogy of human crowd with gases and fluids is justified. In [34, 35] an investigation of pedestrian dynamics with help of the Maxwell-Boltzmann gas theory was presented. In [25] a similar model

was developed but taking into account that, unlike to matter momentum and energy conservation are not guaranteed in a human crowd.

To sum up macroscopic models can be useful in extreme crowded situations and important questions can be answered with a useful precision, e.g. on the average how much is the outflow? But the influence of individuals is neglected. Thus, the ability of macroscopic models to describe less dense situations is questionable.

1.3 Microscopic models

In contrast to the macroscopic models microscopic ones are based on the idea that the dynamics of the crowd emerges inevitably from the movement of individuals. In other words, specifying the properties of individuals and defining their interactions is sufficient to predict and infer the state of the crowd. This "reductionism" should be interpreted with caution, since the whole is not necessary equivalent to the sum of the parts. Later on we will show the existence of phenomena on a large scale, that still can not be described in a satisfactory manner by microscopic models (stop-and-go waves, turbulences).

With respect to observables like space, time and state variables one can classify microscopic models in discrete, continuous or mixed models. The most elaborated classes of models for pedestrian dynamics are rule-based models discrete in space (*cellular automata*) [20, 3, 51, 59, 77, 97], *force-based* models [33, 82, 61, 67, 106, 10, 114, 112, 111, 58, 17, 73, 72], where the trajectories of pedestrians are defined by a system of Ordinary Differential Equations (ODE), *rule-based* models *continuous* in space [117, 99, 2, 9, 119, 107, 78, 103], defined through a set of rules describing the reaction of pedestrians to their surrounding and finally *hybrid* models that incorporate as well forces as rules [130, 85].

The distinction between "force-based" and "rule-based" is difficult, sometimes even impossible to maintain. That has several reasons. First, this terminology is

in pedestrian dynamics not well-established. That means there is no consensus on its definition and meaning. Second, as the investigation in Chap. 2.1 shows, most models that are based on the Newtonian dynamics incorporate *rules* to overcome some side-effects and problems intrinsic to the main equation of movement. In this work we mean with "force-based" models those where the described dynamics is mostly dominated by the defined forces. We define "rule-based" models as such where the space of the decisions that affects the state variables is discrete.

1.3.1   Rule-based models discrete in space: Cellular automata

For simplicity of exposition we restrict ourselves in this section to Cellular Automata (CA). CA can be defined as follows: "CA are mathematical idealizations of physical systems in which space and time are discrete, and physical quantities take on finite set of discrete values." [123]. Many complex systems have been described with CA, e.g. biological systems [65, 36] and vehicular traffic [8]. Despite their complexity it turns out that CA can describe fairly well some of the phenomena emerging from those systems with few simple local rules.

A CA model consists of a regular lattice, usually with cell's size of $40 \times 40 \, \text{cm}^2$. Each cell is described by a discrete variable; "1" for occupied and "0" for empty. The status of CA evolves in discrete time steps $n = 0, 1, 2, \cdots$. The state of one cell is affected by cells in its "neighborhood". Depending on the system different neighborhoods can be defined. Fig 1.2 depicts schematically three of the most common neighborhoods used in CA applied to pedestrian dynamics. Given a cell uniquely determined by its center point (x_0, y_0) and edge length l, one can give following definitions:

- **Von-Neumann neighborhood** defined in a regular grid by

$$\mathcal{N}_n = \left\{ (x, y) : (x - x_0)^2 + (y - y_0)^2 = l^2 \right\}.$$
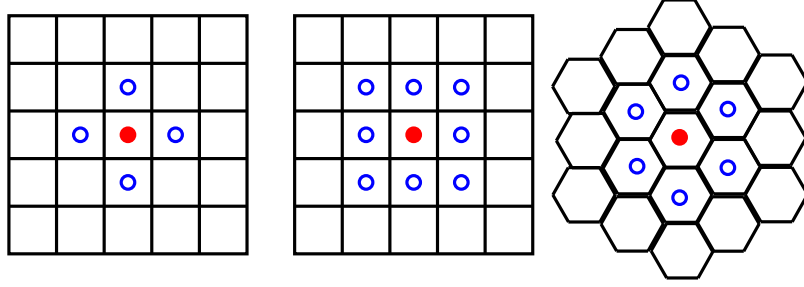
Figure 1.2: Left: Von-Neumann neighborhood. Middle: Moore neighborhood. Right: Hexagonal neighborhood.

Probably this is the most adopted neighborhood in CA models [6, 124, 128].

- **Moore neighborhood** defined in a regular grid by

$$\mathcal{N}_m = \{(x, y) : (x - x_0)^2 + (y - y_0)^2 \leq 2l^2\}.$$

The F.A.S.T-model [59] implements Moore neighborhood for pedestrians moving with a maximal velocity of 1 cell/s.

- **Hexagonal neighborhood** defined by

$$\mathcal{N}_h = \{(x, y) : (x - x_0)^2 + (y - y_0)^2 \leq 5l^2\}.$$

Although not very popular, hexagonal neighborhood was used successfully in [19, 23, 54, 16].

The update procedure from time step n to $n+1$ of the state of a cell is performed according to the states of the neighboring cells, a given order of update and with respect of a definite set of (stochastic) rules.

The order of update is crucial for the dynamics induced by a CA. One can distinguish between at least four basic procedures to fulfill a transition from step n to $n + 1$. Probably the most simple way is to update *sequentially* the state of cells in

a given order. Another form of update procedure is *random-sequential*. Here cells to be updated are chosen randomly without any predefined order. A third update possibility is called *sublattice-parallel* update, where cells belonging to a given lattice are updated simultaneously. Finally, it is possible to update cell state in *parallel* [100]. In [89] the influence of each update on the results of the ASEP-Model was investigated.

1.3.2 Force-based models

One important class of models for pedestrian dynamics are force-based models. These models are motivated by the observation that the motion of pedestrians deviates from a straight path in the presence of other pedestrians. Therefore their motion is accelerated which according to Newton's laws implies the existence of a force.

Force-based models take Newton's second law of dynamics as a guiding principle and profit from a rich theory of dynamical systems as well as well-known numerical solvers for integrating ODE.

Strictly speaking, forced-based models induce some *causality* claims in a deterministic world-view. Pedestrian movement depends only on the initial values of the system they are defined within. However, in general the internal state of pedestrians, which influences their movement, is not considered. Therefore, some models try to compensate this lack by introducing noise and fluctuations.

Given a pedestrian i with coordinates $\overrightarrow{R_i}$ one defines the set of all pedestrians that influence pedestrian i at a certain moment as $\mathcal{N}_i$ and the set of walls or boundaries that act on pedestrian i as $\mathcal{W}_i$. In general the forces defining the equation of motion are split into driving and repulsive forces. The repulsive forces model the collision-avoidance performed by pedestrians and should guarantee a certain volume exclusion for each pedestrian. The driving force, on the other hand, models the intention of a pedestrian to move to a certain destination and walk with a desired speed.

Formally the movement of each pedestrian is defined by the equation of motion

$$m_i \ddot{\overrightarrow{R_i}} = \overrightarrow{F_i} = \overrightarrow{F_i}^{\text{drv}} + \sum_{j \in \mathcal{N}_i} \overrightarrow{F_{ij}}^{\text{rep}} + \sum_{w \in \mathcal{W}_i} \overrightarrow{F_{iw}}^{\text{rep}}, \qquad (1.1)$$

where $\overrightarrow{F_{ij}}^{\text{rep}}$ denotes the repulsive force from pedestrian j acting on pedestrian i, $\overrightarrow{F_{iw}}^{\text{rep}}$ is the repulsive force emerging from the obstacle w and $\overrightarrow{F_i}^{\text{drv}}$ is a driving force. m_i is the mass of pedestrian i.

The time evolution of the non-linear dissipative differential equations (1.1) given particular initial conditions is represented by trajectories in the space of the state variables.

Some seminal works [90, 91, 86] in traffic dynamics studied the movement of cars by means of a system of ODE, describing the change of the state variables in time. Following Newtonian dynamics, action of forces is considered as *cause* of change of the state variable of an object. In other words, changes of the velocity (and space) in time are induced by the existence of forces. As a result, thus the origin of force-based modeling can be traced back to the beginning of the 50's. In 1977 Hirai and Tarui [37] presented a force-based model to desscribe the movement od a crowd in a "panic" situation. Another explicit consideration of this forced-based principle to pedestrian dynamics was probably initiated in 1985 by Gipps et al. who presented a CA model that "hypothesizes the existence of repulsive forces between pedestrians so that as the subject approaches another pedestrian the 'potential energy' of his position rises and the 'kinetic energy' of his speed drops" [20].

Later, Helbing tried in [24] to model the "behavior" of pedestrians. This work can be considered as the basis of the Social Force Model (SFM) [33] which has been published four years later. At this point we would like to mention that the use of the word "behavior" in this context is misleading because the proposed model considers only the operational process of movement, not the causes or stimuli that produce it.

One can argue, that the model [24] comprises the kind of behaviorism represented by Skinner [110]; i.e. human behavior is restricted to what is publicly observed, let's say external action or movement. Internal processes, like thinking, perceiving and feeling, are considered to be irrelevant and does not fit within the concept of "behavior". This kind of *radical behaviorism* is being increasingly dismissed by cognitive scientists, since behavior is hardly to be explained without reference to mental processes. Despite, there is no doubt about the significance of the SFM for force-based modeling of pedestrian movement on an operational level.

In the SFM the repulsive force is described by means of a negative potential with elliptical equipotential lines. Although the repulsive force is symmetrical in space, i.e. pedestrians in front and behind exert the same force, and computationally very intensive (exponential function), the SFM reproduces several qualitative characteristics of pedestrian dynamics, e.g. the formation of lanes in counterflow. Nevertheless various improvements of the original SFM were suggested to overcome the problems encountered. In [29] a more realistic form of the forces was introduced which reflects the anisotropic character of the interactions. Furthermore this generalized SFM takes into account repulsive forces that emerge when pedestrians have physical contact or get too close to each other. Lakoba et al. [61] pointed out other problems like the unrealistic choice of parameters which e.g. leads to extreme physical forces of 6000 N. The problem of the parameter choice in the SFM was again addressed in [47] by calibration based on an evolutionary optimization algorithm. Parisi et al. [82] investigated the difficulties of SFM concerning quantitative description of pedestrian dynamics by introducing a "respect mechanism". This rule-based mechanism helps to mitigate overlapping among pedestrians.

Recently in [108] the human collective behaviors was studied by means of a force-based model inspired by the dynamics of non-human organisms such ants. Needless to say that similarities between human and non-human dynamics were always a source

of inspiration for several models, e.g. the floor-field model [51].

1.3.3   Rule-based and hybrid models

The paradigm of force-based models may become inapt to cover the complexity of human behavior. That led to several attempts at describing interactions among pedestrians and their movement by means of operational "instructions" or rules that specify how state variables or/and specific parameters of a pedestrian should be updated. In that way predictive and explanatory informations about the dynamics of the system can be gained. The granularity of such instructions reflects the complexity of human movement.

In some works both paradigms, namely forced-based and rule-based, were combined to formulate a model. Yu et al. [130] proposed a new model based on forces and rule-based conflict management. The CFM considers both the headway $\overrightarrow{R_{ij}} = \overrightarrow{R_j} - \overrightarrow{R_i}$ and the relative velocity $v_{ij} = v_j - v_i$ among pedestrians in the specification of the force:

$$\overrightarrow{F_{ij}}^{\text{rep}} \propto f(v_{ij}, \| \overrightarrow{R_{ij}} \|^{-1}) \cdot \frac{\overrightarrow{R_{ij}}}{\| \overrightarrow{R_{ij}} \|} . \tag{1.2}$$

Compared to the SFM, the repulsive force in the CFM reflects several new ideas. Besides the simple form of Eq. (1.2), the force is anisotropic since its range of influence is reduced to range of vision of pedestrians, which is 180°. This is realized by a proper choice of the function f. Furthermore it takes into account the influence of the relative velocity, i.e. faster pedestrians in front of a slower pedestrian do not affect its movement.

Unlike most force-based models the role of the repulsive force in the CFM is more to avoid collisions among pedestrians by detours than to prevent them. In order to ensure a volume exclusion, the model introduces a set of *rules*.

Another hybrid model [85] that describes the movement of pedestrian according to separated levels was investigated . The low level describes the operational movement

of pedestrians and is based on the SFM, whereas high levels implement tactical and behavioral aspects of the movement e.g., way-finding in buildings, communication between pedestrians. In [12] a similar idea was realized by coupling a high-level finite-state machine, that models pedestrian's perception of space, with a low-level collision avoidance mechanism.

1.4 Experimental investigation and model calibration

1.4.1 Preliminary

Of particular importance are empirical results which not only provide a benchmark for mathematical models and allow their calibration, but can serve as an inspiration for new modeling concepts. For design and evacuation purposes a reliable quantitative investigation is essential. In order to provide an experimental basis for a quantitative model verification, several experiments under laboratory conditions were conducted. In section 1.1 the question about the quality of mathematical models was briefly discussed. In terms of the minimum-description-length principle it is conceivable even preferable to design a model that describes the target system with a minimum of physical parameters. Besides, another important question is how useful is a mathematical model? Should a model be able to describe quantitative as well as qualitative aspects of the described real-world problem? Roughly speaking, can a "bad looking" model asses quantitative aspects of pedestrian dynamics?

To answer this question experimental measurements of characteristic properties of crowds are necessary. On a quantitative level density, velocity and flow are measured. Particular attention was devoted to the phenomenon of lane formation, especially in bi-directional flow. Different works investigated quantitatively this phenomenon e.g. in [42] by application of cluster analysis, in [125] the bond index method was introduced. In [132] is has been distinguished between "stable separated lanes" and

"dynamical multi lanes". By means of a Voronoi method the influence of those different lane forms on the Fundamental Diagram (FD) of bidirectional streams in comparison to unidirectional ones is investigated.

1.4.2 Qualitative and quantitative aspects of pedestrian dynamics

From a macroscopic point of view several collective phenomena emerge from a dynamic human crowd. Most known in the literature are

- lane formation [33, 125, 26, 130, 42, 132]: One of the most important and well observed characteristics of bi-directional streams. This tendency of pedestrians to walk behind each other and thus to build lanes is an attempt to avoid collisions with pedestrians moving in the opposite direction and maximize its own velocity.

- oscillations at bottlenecks [33, 26, 31, 60]: Oscillations occur when a group of pedestrians compete with another group moving in the opposite direction and aiming to pass trough the same bottleneck. It is characterized by the fact that the direction of the flow alternates in different time intervals.

- the "faster-is-slower" effect [61, 79, 81]: It has been stated that the stronger the collective desire to evacuate from a room the higher the tendency of pedestrians to get stacked precluding them to cross the door and restricting the overall evacuation time.

- clogging at exit [74, 127, 27]: Is a circular clustering of a crowd in front of an exit. Is has been distinguished between "social clogging" and "granular clogging" depending on the nature of interactions [79].

The quantitative aspect of a crowd is usually assessed by means of several physical quantities like velocity, flow and density. In this context the direct comparison of those

quantities is relevant. See also the discussion about the FD in section 1.4.4. Following is a brief definition of each quantity:

- The speed is an average over time or over space. Given a time period Δt and a measurement area of length Δx on can write

$$\langle v \rangle_{\Delta t} = \frac{1}{N_{\Delta t}} \sum_{i=1}^{N_{\Delta t}} v_i(t), \tag{1.3}$$

with $v_i(t)$ the instantaneous velocity of the ith pedestrian and $N_{\Delta t}$ the number of measured pedestrians within the time interval Δt (see Fig. 1.3). The spatial mean speed is written as

$$\langle v \rangle_i = \frac{\Delta x}{\Delta t_i}, \tag{1.4}$$

where Δt_i is the time necessary for the ith pedestrian to pass the measurement area.

- The flow gives the number of pedestrians passing a measurement line during a time interval. Given the time necessary Δt for $N_{\Delta t}$ pedestrians to pass the measurement line the flow J is given by

$$\langle J \rangle_{\Delta t} = \frac{N_{\Delta t} - 1}{\Delta t}. \tag{1.5}$$

- The density is is the number of pedestrians per unit of area. In order to determine the density, in general a rectangular area is defined and the number of pedestrians within this area is counted. The instantaneous density at time t is given by

$$\rho(t) = \frac{N}{|A|}, \tag{1.6}$$

with N the number of pedestrian at the moment t that reside within the mea-
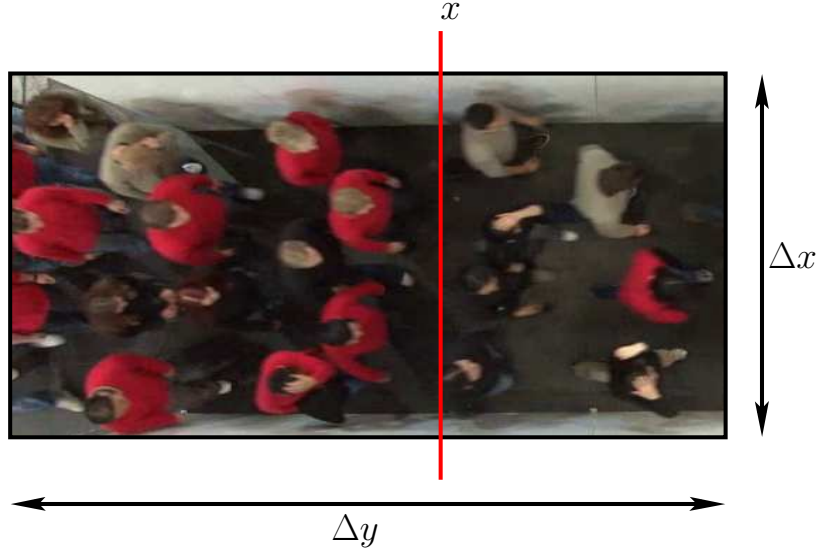
Figure 1.3: Calculating the average of the quantities v, J and ρ by averaging over time or over space; Average of the velocity and flow of pedestrians crossing the line x during a measurement period Δt and the average over the space $(\Delta x \times \Delta y)$ of the velocity and the density. The missing observable cat be calculated using the relation $J \propto v\rho$.

surement area A. $\rho(t)$ can be averaged over a time period Δt as follows:

$$\langle \rho \rangle_{\Delta t} = \frac{1}{\Delta t} \int_{\Delta t} \rho(t)dt. \tag{1.7}$$

As matter of fact the measurement method of each quantity impact the resulting FD and should be taken into consideration while used to calibrate mathematical models. In [101, 132] the advantages and disadvantages of those methods and others were extensively discussed, particularly with regard to fluctuations in empirical data.

1.4.3 Measurement methods of the density

The main problem encountered when measuring the spatial average of the density by means of Eq. (1.6) is the high fluctuations that can be of the same the order of the measured density itself.

Assume N pedestrians reside within the measurement area A at time t. Further-

more, let's assume that at time $t+1$ the number of pedestrians increases by n. The density is then $\rho(t+1) = \rho(t) \pm n \cdot Q$, $Q = 1/|A|$. The function $\rho(t)$ is then a step function of time:

$$\rho(t)\colon \mathbb{R} \to \mathbb{R}$$
$$t \mapsto \frac{N(t)}{|A|}$$

That means the measurement area should be large enough to minimize the scale of the fluctuations, as the quantum Q becomes smaller. However, for a beneficial microscopic modeling and in order to gain microscopic information, the measurement area should be as small as possible, at least about the average size of a human body.

Following, we introduce two methods to overcome those difficulties, concerning the measurement of the density in one-dimensional and in two-dimensional space.

1.4.3.1 One-dimensional pedestrian dynamics

Pedestrian dynamics exhibits a huge amount of rich and complex phenomena. In order to manage its complexity, several factors that have to be dealt with are eliminated by reducing the system to one-dimensional space. In [106] the role of the space requirement of pedestrians in single file movement is investigated. In [9, 88, 87] an event driven model was introduced and developed to investigate the FD and the phenomenon of phase separation in one-dimensional space. Also several experiments in one-dimension were performed to consolidate the experimental database of one-dimensional pedestrian dynamics [105, 7, 46].

Despite the geometric simplicity of one-dimensional systems, several interesting and well known phenomena were showcased by those studies. In [7] an empirical comparison of the FD across different cultures was performed by repeating the same

experiment several times in different countries[1]. In [103, 88] the phenomenon of stop-and-go waves, typical for single-file movement, was investigated experimentally and by simulations.

To avoid the problematical issue of the instantaneous density, Seyfried et al. [105] proposed an enhanced method for measuring the density on single file movement. For each pedestrian one determines its entrance time t_i^{in} to the measurement area and the time t_i^{out} when he leaves it. The density is defined as

$$\rho(t) = \sum_{i=1}^{N} \frac{\Theta_i(t)}{|A_{1d}|}, \tag{1.8}$$

$$\Theta_i(t) = \begin{cases} \frac{t - t_i^{\text{in}}}{t_{i+1}^{\text{in}} - t_i^{\text{in}}} & : \quad t \in \left[t_i^{\text{in}}, t_{i+1}^{\text{in}}\right] \\ 1 & : \quad t \in \left[t_{i+1}^{\text{in}}, t_i^{\text{out}}\right] \\ \frac{t_{i+1}^{\text{out}} - t}{t_{i+1}^{\text{out}} - t_i^{\text{out}}} & : \quad t \in \left[t_i^{\text{out}}, t_{i+1}^{\text{out}}\right] \\ 0 & : \quad \text{else}, \end{cases} \tag{1.9}$$

where $\Theta_i(t)$ gives the fraction of the space between pedestrian i and the pedestrian in its front, which can be found inside the measurement area, $|A_{1d}|$ is the length of measurement area (one-dimensional).

In the classical method, Eq. (1.6), the "contribution" of each pedestrian i to the overall density is binary; 1 if i is within the measurement area, otherwise 0. In the proposed method Eq. (1.8) the contribution of pedestrians is many-valued $\in [0, 1]$. Thus, it reflects better the impact of the actual situation of pedestrians on the density. Meanwhile, the fluctuations are reduced.

1.4.3.2 Two-dimensional pedestrian dynamics

In [113] a method for calculating ρ with help of Voronoi diagrams was introduced. For this Steffen et al. presented a method to calculate a density distribution $p(\overrightarrow{x})$

---

[1]The first experiment was performed in Germany [105] and the second in India [7].

instead of the averaged density. At a given time t, the positions of pedestrians define a unique partition of the space by means of Voronoi diagrams. To each pedestrian i belongs a Voronoi-cell A_i. With those cells one can define a density distribution as follows:

$$\rho_i(\overrightarrow{x}) = \begin{cases} \frac{1}{|A_i|}, & \text{if } \overrightarrow{x} \in A_i \\ 0, & \text{otherwise.} \end{cases}$$

The density inside the measurement area A is

$$\rho(t) = \frac{\displaystyle\int_A p(\overrightarrow{x}) d\overrightarrow{x}}{|A|}, \tag{1.10}$$

with $p(\overrightarrow{x}) = \sum_i \rho_i(\overrightarrow{x})$.

With this measurement method it is possible to reduce, without serious side effects, the size of the area and gain insight of the dynamics on the microscopic level. Furthermore, the fluctuations of the density are diminished [63, 133, 132, 131]. Note that theoretically with the classical definition of the density (1.6), it is not possible to reduce the size of the measurement area without strengthening the fluctuations of the measurements.

1.4.4 Fundamental diagram

The FD depicts the variation of the flow in dependence of the density $J(\rho)$. Other equivalent variations of the FD e.g. $v(\rho)$ and $v(J_s)$ follow from the the hydrodynamic relation

$$J_s = \rho v. \tag{1.11}$$

J_s is the specific flow per unit width w $(J_s = J/w)$.

It describes the transport properties of systems of driven particles. Hence, it is widely considered as a criterion for the correctness of mathematical models for

pedestrian dynamics and is used to calibrate and validate them [68, 13, 106, 10]. In some works [52, 15] the FD is considered as part of the model and not as a benchmark to check against. For this purpose the most cited FD given by Weidmann [121] is used:

$$v = v_0 \cdot \left(1 - \exp\left(-\gamma \cdot (\frac{1}{\rho} - \frac{1}{\rho_{\max}})\right) \right), \tag{1.12}$$

with $\gamma = 1.913\,\mathrm{P/m^2}$, $v_0 = 1.34\,\mathrm{m/s}$ and $\rho_{\max} = 5.4\,\mathrm{P/m^2}$. Certainly the FD plays an important role in pedestrian dynamics. Nevertheless there is an open discussion about the collected empirical data that appears in some cases to be contradictory. More often data used for measurements are not compatible, e.g. the FD given by Weidmann comprehend measurements from unidirectional and bidirectional streams. See [95] and [101] for a more extensive analysis. Despite the discussion about the validity of the collected data, there is an unanimity that the velocity diminishes with increasing density.

1.5 State of the art of experimental investigation of pedestrian dynamics

As the crucial part of any reasonable scientific approach is validation and verification of the hypothesis and/or models that try to give an explanation of the observed phenomena, several experiments under controlled laboratory conditions were prepared and realized. Therefore a detailed quantitative evaluation of the mathematical models was possible. But why should a scientist investigating the field of pedestrian dynamics be interested in controlled experiments under laboratory conditions?

There are various reasons for this issue. First, with records from surveillance cameras installed e.g. in railway stations and buildings it is rather often not possible to extract microscopic trajectories at high quality in space and time. This is mainly due to different factors like the perspective view of the camera, light conditions, etc.

Second, with help of controlled experiments it is possible to study the influence of different geometry specific parameters, e.g. the width of bottlenecks and corridors. This makes the investigation of the influence of the environment on the dynamics of pedestrians possible. Third and this is maybe the most important reason, is to reduce the complexity of the studied system. For example well prepared experimental environments in basic geometries are useful to study the dynamics of pedestrians and to extract valuable knowledge that can be generalized to more complex geometries.

Despite the fact that the experimental data basis is relatively undeveloped, there are important discrepancies in the extracted data and any comparison between experiments should take this state into account. The reason of this is difficult to determine, since some experiments are poorly documented. However, it was indicated in [7] that cultural factors related to differences in the characteristics that emerge from the empirical data. The discrepancies of reported empirical data can also be lead to human properties related to the attendees of the experiments, e.g. age, motivation, homogeneity of the group. Other reasons are more technical and are directly related to the realization of the experiments, extraction of the data and their measurement [104, 132].

In this sense several experiments have been performed to investigate specific issues like flow in bottlenecks, the FD in narrow and wide corridors in comparison to T-junctions.

In this section we give a brief overview of some recent experimental works investigating different issues of pedestrian dynamics.

1.5.1 Single file dynamics without overtaking

Several experimental works tried to eliminate any lateral interactions and boundary effects by studying lane movement dynamics with closed boundary conditions. This approach has the benefit to reduce the complexity of the phenomena that emerge

from the dynamics of pedestrians.

Recently in [46] the instantaneous FD in 1-D movement was measured. It was shown that both stationary and transient phases can be observed. As the main result of those experiments it was observed that the "velocity–spatial headway" relation obeys three different regimes, free, weakly constrained and strong constrained, where the relation is piecewise linear. Those results are in accordance with experiments performed in [105] that showed linearity of the velocity–spacial headway in the "strong constrained" regime.

This empirical finding is quite important for mathematical modeling, as several models assume that the volume exclusion of pedestrians depends linearly on the velocity [106, 9, 87]. It would be interesting to distinguish, on a the modeling level, between the different regions in the velocity–spacial headway relation.

Comparison of similar experiments performed in Germany [105] and India [7] show some cultural influences on the way pedestrians react on each other. In this sense, another experimental study of 1-D movement was presented in [66] with the following result: In comparison to [105, 7], for the same density values higher velocities were observed. In the authors' opinion, this discrepancy could be ascribed to "different body sizes". This explication is hardly comprehensible, since in previous experiences [105, 7] the attendees were students with average body size and thus large differences in the body size can not be assumed.

1.5.2 Wide and narrow corridors with overtaking

Several experiments in straight corridors, where pedestrians could move laterally were conducted in order to study the FD in dependence of various corridor widths. In [133] the FD in straight corridors with open boundary conditions was investigated. Different widths of the corridor were tested. In agreement with Hankin's findings [22] the FD for the same type of facility can be unified into one diagram for specific flow.

In [132] the same kind of experiments in straight corridors were shown, but ordering in bidirectional pedestrian streams was investigated. Furthermore, a classification of bi-directional streams was introduced and their influence on the flow was investigated.

Further bi-directional flow experiments were contacted in [115] focusing on the role of anticipation in mitigating conflicts. The attendees anticipation was varied from weak, normal to excessive. Results of those experiments show that lane formation is more natural in case of normal anticipation. It takes longer in the case of excessive anticipation, but then the lanes formed are more stable. In the case of weak anticipation the number of collisions is higher and thus the evacuation time is long.

1.5.3   Bottlenecks and T-junctions

Bottlenecks and T-junctions are two basic geometries that have attracted special interest in the community of pedestrian dynamics. This can be traced back to the interesting phenomena that emerge from those kind of geometries.

A large set of experiments was conducted in [41] to study the movement of pedestrians at bottlenecks. In those experiments the swaying of pedestrians was measured. It could be found, that the amplitude of swaying decreases with increasing velocity. In contrary, the frequency of swaying increases with increasing velocity. Furthermore, one could also conclude that the flow is a step-function of the bottleneck's width.

Concerning the increase of the flow in dependence of the width of the bottleneck, further experiments were conducted in [57]. As a result Kretz et al. found that the flow increases *linearly* with the width. Therefore, the assumption that the flow is a step function of the bottleneck's width could not be confirmed. In this experimental work also the specific flow was investigated in dependence of the motivation as well as the initial density.

In the same spirit other bottleneck experiments were performed in [102]. Time

evolution of velocity, density and flow were measured. Here again, it was shown that the relation between the flow and the width of the bottleneck is linear.

Further experimental results were presented in [63] with the aim to investigate a wide range of bottleneck specific parameters like length and width of the bottleneck. This allows to study the dependence of the outflow on the length and the width of the bottleneck and confirms the previous results. A phenomenon of side-stepping occurs when the length of the bottleneck is short. This leads to lower densities in front of the bottleneck and hence increased velocities. In [64] an expansion of this work studied the influence of the placement and dimension of the measurement area on the density.

Another experimental study [14] investigated the capacity of emergency doors with the intention to allow an empirical verification of the threshold value in the building decree in Holland. In fact, most experiments they conducted show a higher capacity than expected. An important result of those experiments is the observation that pushing leads to higher velocity. Therefore, the "faster-is-slower" effect could not be confirmed.

The difficulty to correctly model the dynamics of pedestrians in bottlenecks is mainly due to conflicts in front of the exit and how pedestrians deal with them to filter into the bottleneck. In [126] several experiments of bottleneck situations show interesting results. First, the outflow diminished in situations where conflicts among pedestrians becomes relevant. Second, putting an obstacle in front of the exit increases the outflow. According to the authors, the obstacle decreases the number of conflicts, which explains the increased flow.

Finally, Nagai et al. [75] explored dynamical evacuation scenarios, like earthquake or smoky rooms, where people can not any more walk normally by standing. Here again the experiments showed that the flow depends linearly on the width of the exit.

A T-shaped channel or a T-junction is in principle another form of bottlenecks, where two different flows in opposing directions meet at the exits and unify to a

main flow. In [131] experimental results in straight corridors and a T-junction were discussed. By mean of a measurement method based on Voronoi diagrams it was possible to observe a boundary-induced phase transition. A comparison between straight corridor and T-junction indicated that the FDs for different facilities are not comparable. What does this very important result mean for modeling pedestrians dynamics? Especially for modeling works which focus on investigating different geometries, optimally with one set of parameters, this means that this goal may not be possible to achieve and parameters should be adapted to each different geometry, unless the models incorporate boundary effects and geometrical factor in their definition.

1.5.4 Further experiments and field studies

Some experiments were conducted without any geometrical focus in background. In [71] experimental data were collected in order to calibrate the force-based model [33]. Furthermore, with a suitable mathematical (exponential) function the gained experimental data were fitted. Thus, the repulsive force between pedestrians is "not prefabricated" but emerges from a fitting procedure. However, it is not clear if the chosen function gives the *best* fit or its choice leans on the already published models [27, 79, 80, 61, 47, 129]. Besides, it is controversial if the measured interactions between *two* pedestrians can still be guilty for *several* pedestrians, since the superposition principle is not unconditionally extendable to pedestrian dynamics. Moreover, quantitative validation of the calibrated model was missing.

The presented experiments were all conducted in the 2-D plain. In [5] the FD for stairs was extracted from controlled experiments as well as from field studies performed in a football stadium in Düsseldorf (Germany). The gained data were compared to FDs from well-known planning handbooks for pedestrian facilities and evacuation routes. It was found that densities higher than 3.5 m^{-2} were not observed. A concluding result of this work is that values for maximal flow in most hand books

is optimistic. For security planing, smaller values should be taken into account.

Another interesting field study was described in [32]. This study is based on video analysis of the Muslim pilgrimage in Mina/Makkah. The results show that in average local speeds and flows do not vanish no matter how high is the level of the crowdedness.

CHAPTER II

Restrictions of state variables and collision management in force-based models

2.1 Introduction

Most of force-based models describe pedestrian dynamics qualitatively fairly well. Collective phenomena like lane formation [33, 26, 130], oscillations at bottlenecks [33, 26], the "faster-is-slower" effect [61, 81], clogging at exit doors [26, 130] are reproduced. Unfortunately there are only poor quantitative descriptions of these phenomena or in case of the "faster-is-slower" effect a convincing experimental evidence is still lacking.

For practical and critical application a reliable quantitative investigation is essential. In section 1.4 we have presented a brief overview of some experiments, that were conducted in the past. They offer more experimental insights to understand the dynamics of pedestrians and serve as validation and verification tool for mathematical models.

Most force-based models contain free parameters that can be adequately calibrated to achieve a good quantitative description [44, 47, 58, 82, 40]. In most works quantitative investigations of pedestrian dynamics were restricted to a specific scenario or geometry, like one-dimensional motion [9, 106, 103], behaviour at bottlenecks

25

[58, 43, 41], two-dimensional motion [82] or outflow from a room [51, 50, 49, 126]. In more complex scenarios e.g. a building where all "basic" geometries (corridors, bottlenecks, corners, ...) and their variants can be found, it becomes more challenging to calibrate a model that describes the dynamics in the complete building correctly.

Usually, implementations of the repulsive force require additional elements to guarantee realistic movement, especially in high density situations. One serious problem is overlapping of the geometrical forms presenting pedestrians, e.g. circles, ellipses [61, 130]. Another problem is negative and unrealistically high velocities that can be produced while a simulation [33, 67] occur as artefacts of the force-based description. This then has to be rectified by supplementing the equation of motion (1.1) with other procedures, e.g. collision detection algorithms. This increases the complexity of the model. Sometimes the additional procedures are not well documented which can lead to misinterpretation of the model. In [11] it was shown that algorithms for collision detection and avoidance can dominate the dynamics and mask the role of the repulsive force.

Furthermore, this approach is clearly contradictory to the principle Occam's razor, since some elements of the model can become redundant or even superficial. This point will be elaborated in section 2.3.

2.2 Intrinsic problems of force-based models

2.2.1 The "*actio et reactio*"-principle

As mentioned earlier the force-based modeling approach of pedestrian dynamics is based on Newtonian dynamics. Paradoxically some principles of the latter are conceptual problems of force-based models for pedestrian dynamics. The first problem is Newton's third law. According to this principle two particles interact by forces of equal magnitudes and opposite directions. For pedestrians this law is unrealistic since
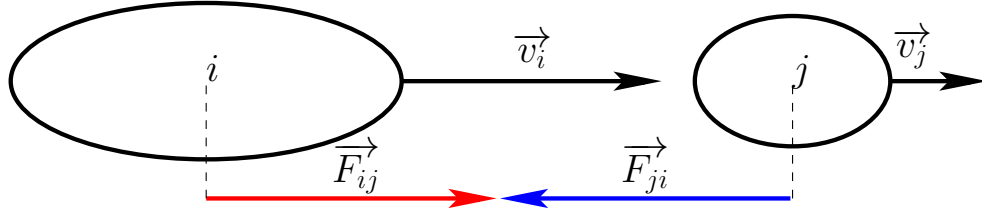
Figure 2.1: Illustration of the "*actio et reactio*"-problem. Pedestrian j exerts a repulsive force on pedestrian i. Meanwhile a repulsive force with the same magnitude and opposite direction acts upon his/her body and pushes him/her forward.

e.g. in general a pedestrian does not react to pedestrians behind him/her. Even if the angle of vision is taken into account, the forces mutually exerted on each other are not of the same magnitude so that the "*actio et reactio*"-principle does not hold in pedestrian dynamics. In Fig. 2.1 a simple scenario illustrate the side-effect of the "actio et reactio"-principle. Pedestrian i moves faster than pedestrian j. By means of a repulsive force that the later exerts on the first, this get slower and in optimal case ends by adapting it velocity to the velocity of its predecessor. However, pedestrian j get pushed by pedestrian i, since he/she will be influenced by the same repulsive force but with opposite direction. In some crowd scenarios, it may be realistic to get pushed by people behind. However, this can not be generalized to all possible situations.

2.2.2 The superposition principle

The second problem emerges from the superposition principle, according to which the total force acting on a particle is given by the vector sum of the individual forces. This principle is valid in physics and systems theory for all linear systems. However, for force-based models describing pedestrian dynamics this can lead to undesired effects, especially in dense situations where unrealistic backwards movement or high velocities can occur.

This problem becomes more serious with increasing range of the forces. Most
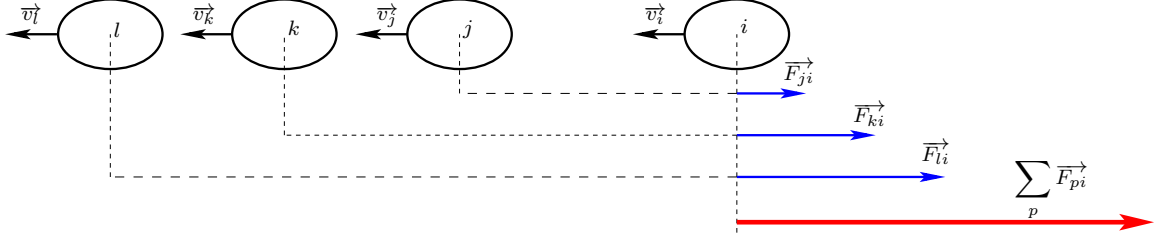
Figure 2.2: Illustration of the superposition-problem in a one-dimensional scenario. Between i and k as well as l there is no visual contact. However, i is influence by their presence.The Force acting on i results from summing the influence of all pedestrians, which may lead to critical values of state variables.

force-based models consider a long-range force. In [28, 81, 82] an exponential-like function was considered. In [33, 106, 30, 130, 10] a function inversely proportional to the distance of two pedestrians was introduced. Although in some works the range of the forces was explicitly reduced to a certain cut-off radius.

Let's consider the case where the repulsive force between two pedestrians i and j takes the form $\overrightarrow{F_{ij}} \propto \dfrac{1}{r}$, with r the distance between i and j. Without loss of generality we can assume that the motion of the pedestrians can be compared to the motion of particles and thus ignore their volume. In this case we consider a half circle of radius r which center coincides with the center of i. Theoretically, on the half circle on can count $\pi \cdot r$ particles. Because of the superposition principle the cumulative force that exerts on i is:

$$\sum_{j \neq i} \overrightarrow{F_{ij}} \propto \pi \cdot r \cdot \sum_{j \neq i} \frac{1}{r} \propto \pi.$$

That implies, the resulting force is constant and does not depend on the distance. For $r \to \infty$ one would expect no influences on i. However, the contribution to the force remains constant, which is contradictory to logical expectations.
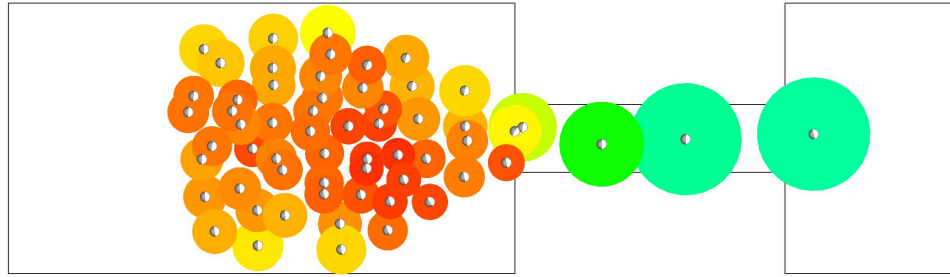
Figure 2.3: Evacuation from a bottleneck. The simulation screenshot highlights the problem of excessive overlapping.

2.2.3 Overlapping and oscillations

Further problems are related to the Newtonian equation of motion describing particles with inertia. This could lead to overlapping and oscillations of the modeled pedestrians. Depending on the strength of the repulsive forces the geometrical form modeling the two-dimensional projection of the human body can be excessively overlapped and violate the principle of volume exclusion[1]. In dense situations small overlaps could be acceptable and be interpreted as "elastic deformations" of the body. However, large overlaps or even inter-penetrations are clearly unrealistic (Fig. 2.3).

Oscillations occur in force-based models because pedestrians do not stop and keep moving independently of the actual situation. It can not be excluded that in some situations pedestrians perform repetitive backwards and forwards movement due to e.g. high repulsive forces. In general we say oscillations occur if pedestrians fulfil backwards movement. In Fig. 2.4 one sees how pedestrians are steering in the wrong direction (white half ellipse stands for the face).

Avoiding overlapping between pedestrians and oscillations in their trajectories is difficult to accomplish in force-based models. On one hand, increasing the strength of the repulsive force with the aim of excluding overlapping during simulations leads

---

[1]In CA-Models this principle is guaranteed by a maximum cell-occupation number.
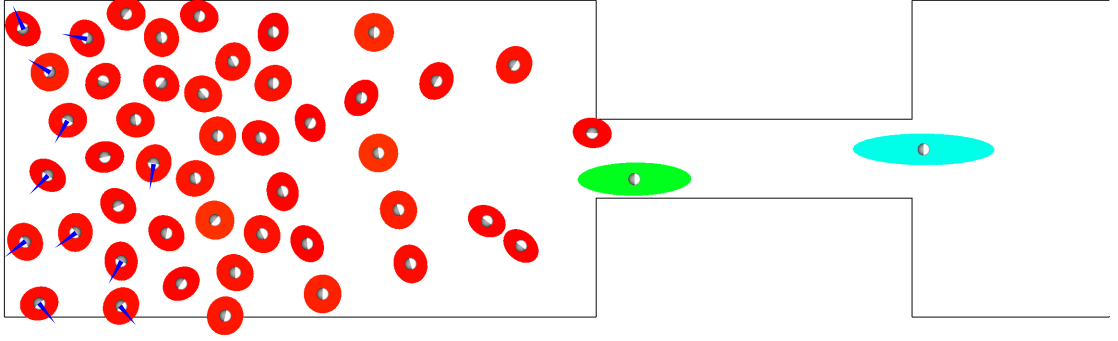
Figure 2.4: Evacuation from a bottleneck. The simulation screenshot highlights the problem of oscillations. Remark the pedestrian in the crowd and near the walls have the wrong orientation.

to oscillations in the trajectories of pedestrians. Consequently backward movements occur which is not realistic especially in evacuation scenarios. On the other hand, reducing the strength of the repulsive force (to avoid oscillations) leads to an increase of overlapping between pedestrians or between pedestrians and obstacles.

2.3 Collision management in force-based models

In this section we discuss the effects of collision management on the dynamics of a system described by a force-based model. After calculating the actual forces the equation of motion is solved at time $t + \Delta t$ to yield for each pedestrian i new state variables

$$\begin{pmatrix} \overrightarrow{R_i}(t + \Delta t) \\ \overrightarrow{v_i}(t + \Delta t) \end{pmatrix} = \int_t^{t+\Delta t} \begin{pmatrix} \overrightarrow{v_i}(t) \\ \overrightarrow{F_i}(t)/m_i \end{pmatrix} dt + \begin{pmatrix} \overrightarrow{R_i}(t) \\ \overrightarrow{v_i}(t) \end{pmatrix}. \tag{2.1}$$

This procedure is repeated as many times as necessary. If using some supplementary rules, the result of the force-based model according to the Eq. (2.1) is manipulated. This could be the case if the state variables take erroneous values e.g., high velocities $(\| \overrightarrow{v_i} \| \gg \| \overrightarrow{v_i^0} \|)$, or the exclusion principle is violated.

The CFM [130] is one of the first force-based models that describes clearly a CDT to deal with the problem of overlapping pedestrians. This supplementary collision management can be interpreted as a failure of the avoidance mechanism expressed in form of repulsive forces. In this sense, the formulation of a repulsive force that theoretically should guarantee a certain volume exclusion is not consistent with a further method to manage collisions and in fact do the same task.

To examine this redundancy we simulate the movement of $N = 180$ pedestrians through a bottleneck. By changing constantly the width of the bottleneck we measure the flow using formula (1.5). For our simulations we use the CFM [130]. Recall, the CFM is a force based-model that is composed of a driven force, a repulsive force and a CDT. The algorithm of the CDT is depicted in Fig. 2.5. For the sake of demonstration we perform several simulations. At a first step by dispensing with the CDT such that the effects of the forces especially the repulsive force can be observed. At a second step we switch on the CDT and dispense with the repulsive force. In this manner we can exactly differentiate between the impact of each mechanism on the dynamics. To be in accordance with the CFM, we make use in both cases of circles with constant radius of $r = 40$ cm.

In Fig. 2.6 we observe that the flow remains unrealistically high which let us conclude that despite the existence of repulsive forces the amount of overlapping during a simulation is important. This explains the high value of the flow. Thus those results show that the repulsive force in this case has no significant effects on the outcome of the simulation.

In the second part of our investigation we perform the same simulations by only replacing the repulsive force by the CDT. Fig. 2.7 shows that the simulation results are in good accordance with empirical data.

To conclude, we have observed that supplementary algorithms can have a major influence on the behavior of a force-based model. In some cases even they make other
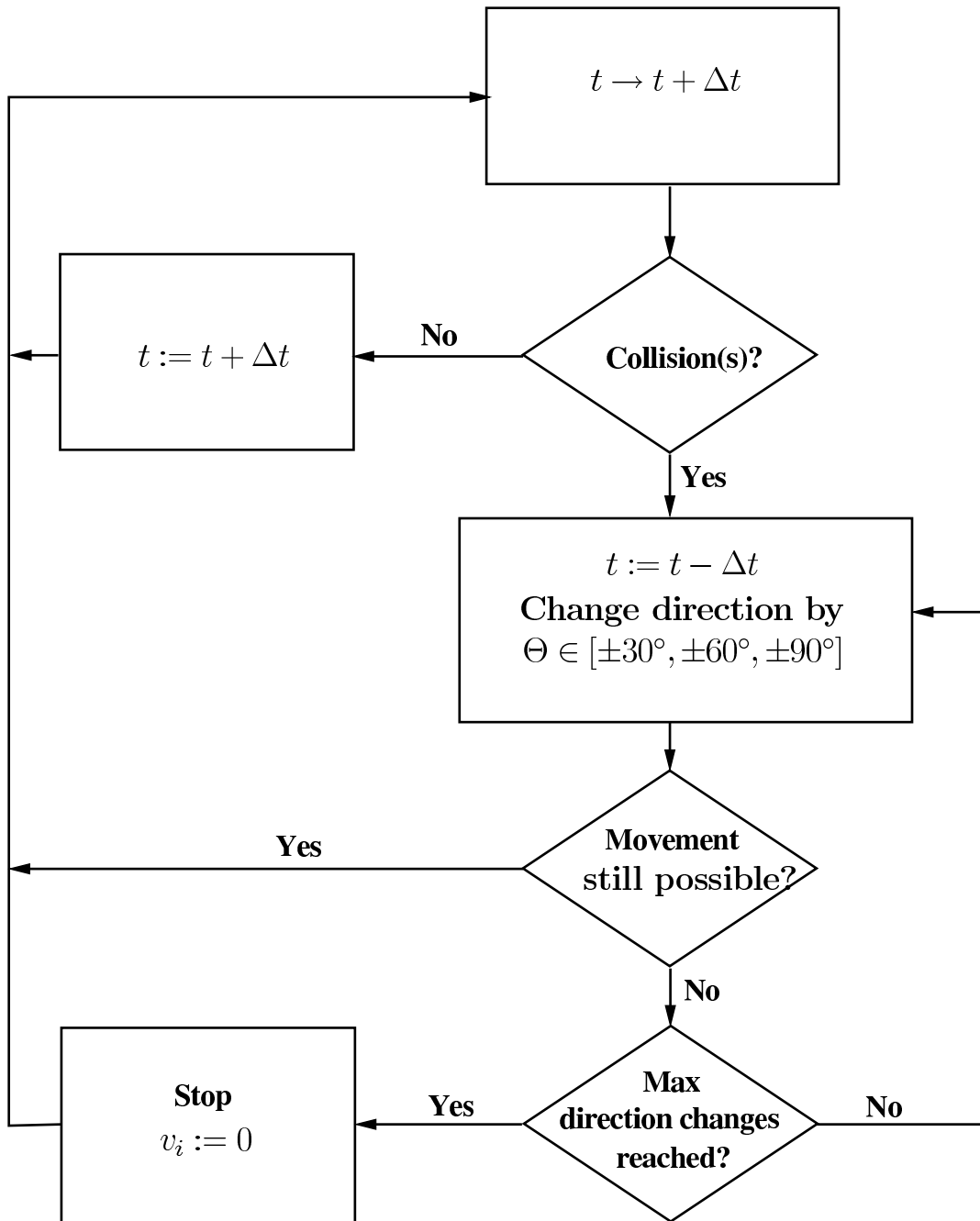
Figure 2.5: Schematic representation of the collision detection technique (CDT), which is an important component in the CFM [130], to manage collisions and mitigate overlapping among pedestrians. In Chap. 3.1 a new model will be introduced that does not rely on the CDT to manage collisions, which is a considerable simplification in comparison to the CFM.
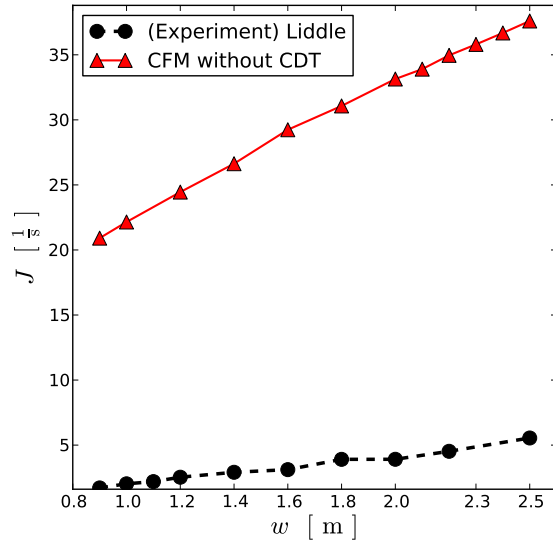
Figure 2.6: Simulations with the CFM without the CDT compared with empirical data from [63].
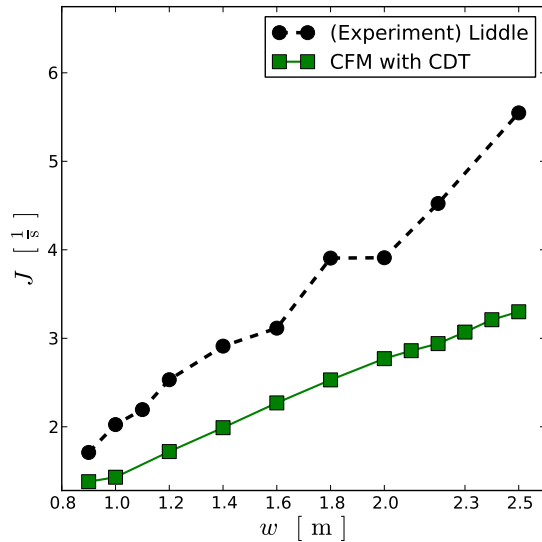
Figure 2.7: Simulations with the CDT but without repulsive forces compared with empirical data from [63].

pivotal components of the model superficial. From a mathematical point of view manipulating the right hand-side of the ODE (1.1) at each time step deteriorates in some cases the stability of the system. This study shows that the volume exclusion is a major factor in every model that aims to describe adequately pedestrian dynamics. In the case of a bottleneck we showed that managing collisions by means of the CDT enhanced the ability of the CFM to guarantee the volume exclusion. As a result the values of the flow became realistic and comparable to the experimental data.

CHAPTER III

The generalized centrifugal force model

3.1 Introduction

The Generalized Centrifugal Force Model (GCFM) [10] describes the two dimensional projection of the human body, by means of ellipses with velocity-dependent semi-axes. It takes into account the distance between the "edges" of the pedestrians as well as their relative velocities. An elliptical volume exclusion has several advantages over a circular one, since a circle is symmetric with respect to its center. This contradicts the asymmetric space requirement of pedestrians in their direction of motion and transverse to it.

As a force-based model, the GCFM describes the time evolution of pedestrians by a system of superposing short-range forces. Besides the geometrical shape of modeled pedestrians, it emphasizes the relevance of clear model definition without any hidden restrictions on the state variables. Furthermore, the quantitative validation of the model with help of experimental data, taken from different scenarios, plays a key role in the development of the model. We systematically calibrate the free parameters of the model by considering single file movement, two dimensional movement in corridors, bottlenecks and corners.

3.2   The driving force of pedestrians

Let's consider a pedestrian i initially at rest $(t = 0)$. Assuming there are no exterior restrictions that might hinder its free movement, i accelerates towards a given destination. After some time, i keeps moving with a certain velocity $\overrightarrow{v_i^0}$. At this moment its acceleration vanishes, either because it feels comfortable at the reached velocity or its physical capacity does not permit further acceleration. From a mathematical standpoint the acceleration may be of different nature, e.g. Dirac-like, linear or exponential [86]. The later type is more realistic and can take the following expression:

$$\overrightarrow{v_i}(t) = \overrightarrow{v_i^0} \cdot \left(1 - \exp\left(-\frac{t}{\tau}\right)\right), \tag{3.1}$$

with τ a time constant. Fig 3.1 shows the evolution of the velocity with respect to time.
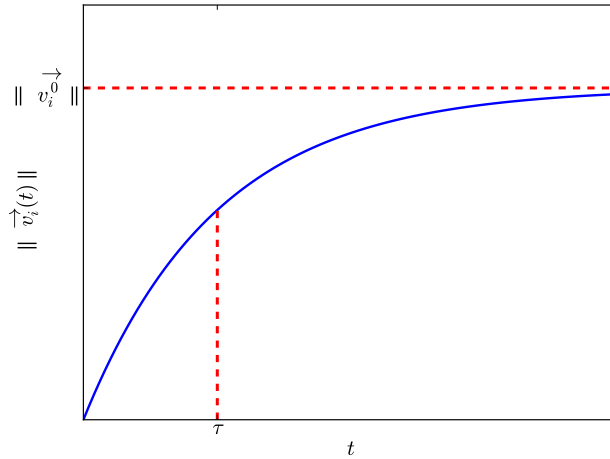
Figure 3.1: Expected evolution of a pedestrian's velocity with respect to time.

Derivation of Eq. (3.1) with respect to t yields

$$\frac{\partial \overrightarrow{v_i}(t)}{\partial t} = \frac{1}{\tau} \cdot \overrightarrow{v_i^0} \exp\left(-\frac{t}{\tau}\right). \tag{3.2}$$

From Eq. (3.1) one gets

$$\vec{v_i^0} \exp\left(-\frac{t}{\tau}\right) = \vec{v_i^0} - \vec{v_i}(t). \tag{3.3}$$

Combining (3.2) and (3.3) and considering Newton's second law, the force acting on i with mass m_i is

$$\vec{F_i}^{\text{drv}} = m_i \frac{\vec{v_i^0} - \vec{v_i}}{\tau}. \tag{3.4}$$

This mathematical expression of the driving force, is systematically used in all known force-based models and describes well the free movement of pedestrians. In [122] is has been reported that evaluation of empirical data yields $\tau = -0.61$ s. A slightly different value of τ was measured in [71] ($\tau = 0.54 \pm 0.05$ s).

3.3   Pedestrian-pedestrian interaction

Assuming the direction connecting the positions of pedestrians i and j is given by

$$\vec{R_{ij}} = \vec{R_j} - \vec{R_i}, \qquad \vec{e_{ij}} = \frac{\vec{R_{ij}}}{\parallel \vec{R_{ij}} \parallel}, \tag{3.5}$$

the repulsive force reads

$$\vec{F_{ij}}^{\text{rep}} = -m_i k_{ij} \frac{(\eta \parallel \vec{v_i^0} \parallel + v_{ij})^2}{d_{ij}} \vec{e_{ij}}, \tag{3.6}$$

with the effective distance between pedestrians i and j

$$d_{ij} = \parallel \vec{R_{ij}} \parallel - r_i(v_i) - r_j(v_j). \tag{3.7}$$

r_i is the polar radius of pedestrian i (Fig. 3.2).
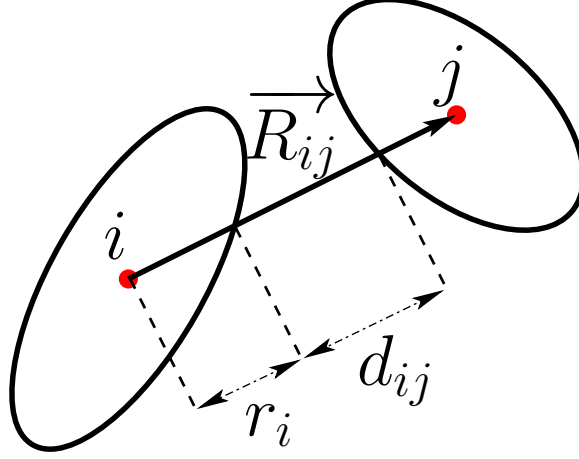
Figure 3.2: Direction of the repulsive force between two pedestrians.

This definition of the repulsive force reflects several aspects. First, the force between two pedestrians decreases with increasing distance. In the GCFM it is inversely proportional to their distance (3.7). Furthermore, the repulsive force takes into account the relative velocity v_{ij} between pedestrians i and pedestrian j. The following special definition ensures that slower pedestrians are less affected by the presence of faster pedestrians than of slower ones:

$$
\begin{aligned}
v_{ij} &= \frac{1}{2}[(\vec{v_i} - \vec{v_j}) \cdot \vec{e_{ij}} + |(\vec{v_i} - \vec{v_j}) \cdot \vec{e_{ij}}|] \\
&= \begin{cases} (\vec{v_i} - \vec{v_j}) \cdot \vec{e_{ij}} & \text{if } (\vec{v_i} - \vec{v_j}) \cdot \vec{e_{ij}} > 0 \\ 0 & \text{otherwise.} \end{cases}
\end{aligned}
\tag{3.8}
$$

As in general pedestrians react only to obstacles and pedestrians that are within their perception, the reaction field of the repulsive force is reduced to the angle of vision

(180°) of each pedestrian, by introducing the coefficient

$$k_{ij} = \frac{1}{2}\frac{\overrightarrow{v_i}\cdot\overrightarrow{e_{ij}}+\mid\overrightarrow{v_i}\cdot\overrightarrow{e_{ij}}\mid}{v_i}$$

$$= \begin{cases} (\overrightarrow{v_i}\cdot\overrightarrow{e_{ij}})/\parallel\overrightarrow{v_i}\parallel & \text{if } \overrightarrow{v_i}\cdot\overrightarrow{e_{ij}} > 0 \ \& \ \parallel\overrightarrow{v_i}\parallel\neq 0 \\ 0 & \text{otherwise.} \end{cases} \tag{3.9}$$

The coefficient k_{ij} is maximal when pedestrian j is in the direction of movement of pedestrian i and minimal when the angle between j and i is bigger than 90°. Thus the strength of the repulsive force depends on the angle.

3.4   Pedestrian-wall interaction

The repulsive force between a pedestrian i and a wall is zero if i performs a parallel motion to the wall. While this behavior of the force is correct, it leads to very small repulsive forces when the pedestrians motion is almost parallel to the wall. For this reason we characterize in this model walls by three point masses acting on pedestrians within a certain interaction range (Fig. 3.3).
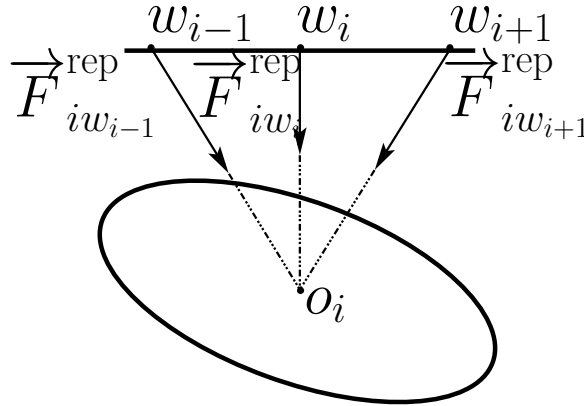
Figure 3.3: Each wall is modeled as three static point masses acting on pedestrians.

The middle point is the point with the shortest distance from the center of the pedestrian to the line segment of the wall. All three points have to be computed at

each step as the pedestrian moves. The distance between the three wall points is set to the minor semi-axis of an ellipse If one lateral point (w_{i-1} or w_{i+1}) does not lie on the line segment of the wall, then it will not be considered in the computation of the repulsive force.

The number of point masses have been chosen by a process of trial and error. Simulations have shown that three point masses are sufficient to keep pedestrians away from walls. Meanwhile they are computationally cost-effective.

As walls are static objects, the repulsive force emerging from a wall w and acting on pedestrian i simplifies to

$$\overrightarrow{F_{iw}}^{\text{rep}} = \sum_{j=i-1}^{i+1} \overrightarrow{F_{iw_j}}^{\text{rep}}, \qquad (3.10)$$

with

$$\overrightarrow{F_{iw_j}}^{\text{rep}} = -m_i k_{iw_i} \frac{(\eta \parallel \overrightarrow{v_i^0} \parallel + v_i^n)^2}{d_{iw_j}} \overrightarrow{e_{iw_j}}, \qquad j \in \{i-1,\, i,\, i+1\}. \qquad (3.11)$$

v_i^n is the component of the velocity normal to the wall, k_{iw_i} and $\overrightarrow{e_{iw_j}}$ as defined resp. in Eqs. (3.9) and (3.5) in Sec. 3.3.

The distance between a line w and the ellipse i is

$$d_{iw} = k_i - r_i, \qquad (3.12)$$

with r_i the polar radius and k_i the distance of point o_i to the line w.

Note that in Eq. (3.11), k_{iw_i} in the force is independent of the chosen lateral wall point w_j. That means, if a pedestrian is moving parallel to the wall, $k_{iw_i} = 0$ and thus the points $j-1$ and $j+1$ have no effects.

3.5 Implementation of the repulsive force

In this section we describe a numerical treatment of the repulsive force. For the sake of simplicity we focus on the case of pedestrian-pedestrian interactions. The pedestrian-wall case is treated similarly.

The strength of the repulsive force decreases with increasing distance between two pedestrians. Nevertheless the range of the repulsive force is infinite. This is unrealistic for interactions between pedestrians. Therefore, we introduce a cut-off radius

$$r_c = 2 \text{ m} \tag{3.13}$$

for the force limiting the interactions to adjacent pedestrians solely. To guarantee robust numerical integration a two-sided Hermite-interpolation of the repulsive force is implemented. The interpolation guarantees that the norm of the repulsive force decreases smoothly to zero for $d_{ij} \to r_c^- = r_c - r_{\text{eps}}$. For $d_{ij} \to \tilde{l}^+$ the interpolation avoids an increase of the force to infinity but to

$$f_m = f_{\max} \parallel \overrightarrow{F_{ij}}^{\text{rep}}(r_{\text{eps}}) \parallel \tag{3.14}$$

at $s_0 = r_{\text{eps}}$ and

$$r_{\text{eps}} = 0.1 \text{ m}, \tag{3.15}$$

where it remains constant. $\tilde{l}$ is the minimum distance between two ellipses and is illustrated in Chap. IV. Fig. 3.4 shows the dependence of the repulsive force on the distance for constant relative velocity.

The right interpolation function P_r and the left one P_l (dashed parts of the function

in Fig. 3.4) are defined using

$$
\begin{cases}
P_r(\tilde{r}_c) = \parallel \overrightarrow{F_{ij}'}^{\mathrm{rep}}(\tilde{r}_c) \parallel, & P_r(r_c) = 0 & (3.16) \\
(P_r)'(\tilde{r}_c) = \left(\parallel \overrightarrow{F_{ij}'}^{\mathrm{rep}} \parallel \right)' (\tilde{r}_c), & (P_r)'(r_c) = 0, & (3.17)
\end{cases}
$$

with $\tilde{r}_c = r_c - r_{\mathrm{eps}}$ and

$$
\begin{cases}
P_l(s_0) = f_m, & P_l(r_{\mathrm{eps}}) = \parallel \overrightarrow{F_{ij}'}^{\mathrm{rep}}(r_{\mathrm{eps}}) \parallel & (3.18) \\
(P_l)'(s_0^+) = 1, & (P_l)'(r_{\mathrm{eps}}) = \left(\parallel \overrightarrow{F_{ij}'}^{\mathrm{rep}} \parallel \right)' (r_{\mathrm{eps}}), & (3.19)
\end{cases}
$$

where the prime indicates the derivative. s_0 is the minimum allowed magnitude of the effective distance of two ellipses. Due to the superposition of the forces the inequality

$$
d_{ij} \geq s_0 \qquad (3.20)
$$

for pedestrians i and j is not guaranteed.

3.6 Quantification of the overlap-oscillation duality

In order to investigate the dual problem of overlapping and oscillations during simulations we introduce two quantities: The overlapping and the oscillation ratios. By means of simulations with different strength of the repulsive force we show that it is difficult to find a value where both ratios vanish.

42
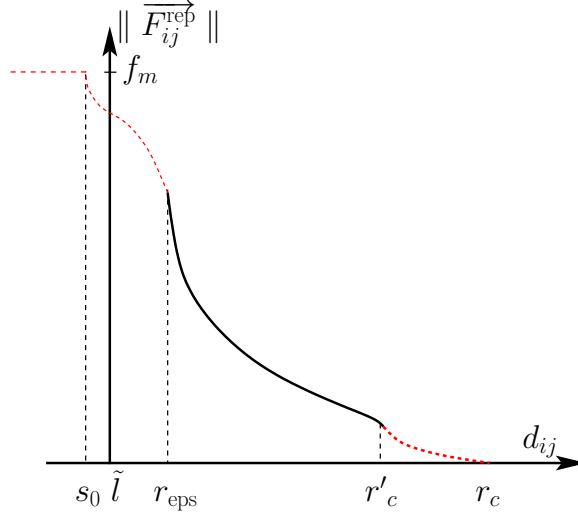
Figure 3.4: The interpolation of the repulsive force between pedestrians i and j Eq. (3.6) depending on d_{ij} and the distance of closest approach $\tilde{l}$, see Chap. IV. As the repulsive force also depends on the relative velocity v_{ij}, this figure depicts the curve of the force for $v_{ij} = \text{const}$. The right and left dashed curves are defined in Eqs. (3.16), (3.17), (3.18) and (3.19) respectively. The wall-pedestrian interaction has an analogous form with d_{ij} and $\tilde{l}$ replaced by d_{wi} and $\tilde{k}$, respectively.

3.6.1 Overlapping ratio

For the sake of convenience we assumed that pedestrians are represented with ellipses. First, we define the overlapping-proportion by

$$o^{(v)} = \frac{1}{n_{ov}} \sum_{t=0}^{t_{\text{end}}} \sum_{i=1}^{N} \sum_{j>i}^{N} o_{ij} , \qquad (3.21)$$

with

$$o_{ij} = \frac{A_{ij}}{\min(A_i, A_j)} \leq 1, \qquad (3.22)$$

where N is the number of simulated pedestrians and t_{end} the duration of the simulation. A_{ij} is the overlapping area of the ellipses i and j with areas A_i and A_j, respectively (3.5).
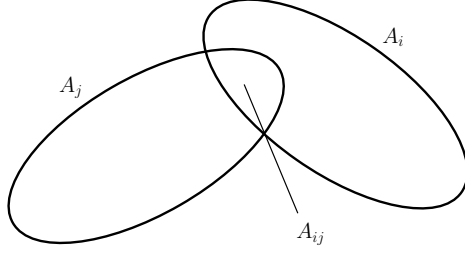
Figure 3.5: Overlapping area of two ellipses.

The algorithm [45] for calculating of A_{ij} analytically is based on the Gauss-Green formula. Since this work is still in process we adopt in this work an numerical approximation, where the ellipse is represented by a 40-sided polygon. Fig. 3.6 depicts n-sided polygons inscribed in an ellipse for $n = 6, 8, 10$ and 40. In App.C we give more details on this approximation and show by means of an error analysis that for sufficiently large n the approximated area of the ellipse is sufficient for the concern of this study.
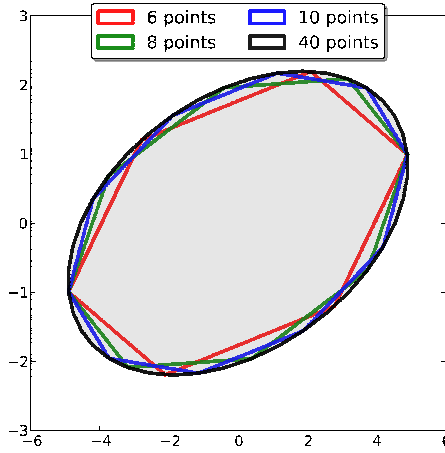
Figure 3.6: Approximation of the ellipse by n-sided inscribed polygons.

n_{ov} is the cardinality of the set

$$\mathcal{O} := \{o_{ij} : o_{ij} \neq 0\}. \tag{3.23}$$

44

For $n_{\mathrm{ov}} = 0$, $o^{(v)}$ is set to zero.

3.6.2 Oscillation ratio

For a pedestrian with velocity $\overrightarrow{v_i}$ and desired velocity $\overrightarrow{v_i^0}$ we define the oscillation-proportion as

$$o^{(s)} = \frac{1}{n_{\mathrm{os}}} \sum_{t=0}^{t_{\mathrm{end}}} \sum_{i=1}^{N} S_i \,, \tag{3.24}$$

where S_i quantifies the oscillation-strength of pedestrian i and is defined as follows:

$$S_i = \frac{1}{2}(-s_i + |s_i|)\,, \tag{3.25}$$

with

$$s_i = \frac{\overrightarrow{v_i} \cdot \overrightarrow{v_i^0}}{\|\overrightarrow{v_i^0}\|^2}\,, \tag{3.26}$$

and n_{os} is the cardinality of the set

$$\mathcal{S} := \{s_i : s_i \neq 0\}. \tag{3.27}$$

Here again $o^{(s)}$ is set to zero if $n_{os} = 0$. The proportions $o^{(v)}$ and $o^{(s)}$ are normalized to 1 and describe the evolution of the overlapping and oscillations during a simulation.

3.6.3 Numerical results

To investigate the behavior of the overlapping ratio (3.21) and the oscillation ratio (3.24) we simulate the single-file movement of $N = 5$ pedestrians. By varying the strength of the repulsive force we measure for each run o^v and $o^{(s)}$. Fig. 3.7 shows the mean value of 200 runs.

Increasing the strength of the repulsive force to make pedestrians "impenetrable" leads to a decrease of the overlapping ratio $o^{(v)}$. After a while, the oscillation ratio $o^{(s)}$ increases, thus the system tends to become unstable. Large values of the oscillation-
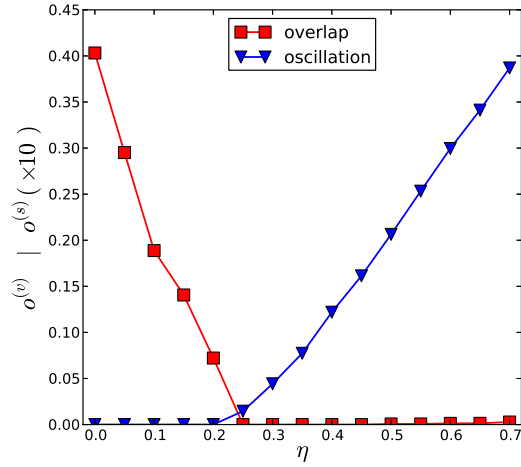
Figure 3.7: The change of the overlapping ratio (3.21) and the oscillation ratio (3.24) in dependence of the repulsive force strength. For each η, 200 simulations were performed.

proportion $o^{(s)}$ imply less stability. For $s_i = 1$ one has $\overrightarrow{v_i} = -\overrightarrow{v_i}^0$, i.e. a pedestrian moves backwards with desired velocity. Since, there are no restriction of the velocity, even values of s_i higher than 1 are not excluded and can occur during a simulation.

Unfortunately, we were not able to adjust the strength of the repulsive force in order to get an overlapping-free model which is at the same time also oscillation-free.

CHAPTER IV

Modeling the shape of pedestrians beyond point like repulsive forces

4.1 Introduction

In this section we investigate the following question: *Does the form of the approximated physical shape of the human body influence the performance and accuracy of a model?*

Force-based models consider the movement of pedestrians as a result of superposing forces, that acts on the center of mass of pedestrians. Therefore it seems to be straightforward that the approach of modeling pedestrians as point-like particles influenced by force fields of other point-like particles do not need to take into account the volume of human bodies. Other models consider circles with constant radius, which is in principle equivalent to point-like particles. However, it was shown in [103, 106] that considering pedestrian as extended objects which change their shape with speed, has several advantages and describe more closely the movement of pedestrians.

One drawback of circles that impact negatively the dynamics is their rotational symmetry with respect to their centers. Therefore, they occupy the same amount of space in all directions. In single file movement this is irrelevant since the circles are projected to lines and only the required space in movement direction matters.

However, in two-dimensional movement the aforementioned symmetry has a negative impact on the movement of pedestrians by occupying unnecessary lateral space.

Other sophisticated form was also investigated. In [117] a "three circle body" was introduced. It is based on three overlapping circles representing the 2-D projection of the body. This form allows in principle easily an assessment of contact between two pedestrians. The same geometrical interpretation of the human body was used in [62] and [53].

In [18] Fruin introduced the "body ellipse" to describe the plane view of the average adult male human body. Pauls [84] presented ideas about an extension of Fruin's ellipse model to better understand and model pedestrian movement as density increases. Templer [116] noticed that the so called "sensory zone", which is a bubble of space between pedestrians and other objects in the environment to avoid physical conflicts and for psychocultural reasons, varies in size and takes the shape of an ellipse. In fact, ellipses are closer to the projection of required space of the human body on the plane, including the extent of the legs during motion and the lateral swaying of the body.

Given a pedestrian i we define an ellipse with center (x_i, y_i), major semi-axis a and minor semi-axis b. a models the space requirement in the direction of movement. We set

$$a = a_{\min} + \tau_a v_i \tag{4.1}$$

with two parameters $a_{\min}$ and τ_a.

Fruin [18] observed body swaying during both human locomotion and while standing. Pauls [1] remarks that swaying laterally should be considered while determining the required width of exit stairways. In [41] characteristics of lateral swaying are determined experimentally. Observations of experimental trajectories in [41] indicate that the amplitude of lateral swaying varies from a maximum $b_{\max}$ for slow movement and gradually decreases to a minimum $b_{\min}$ for free movement when pedestrians

48
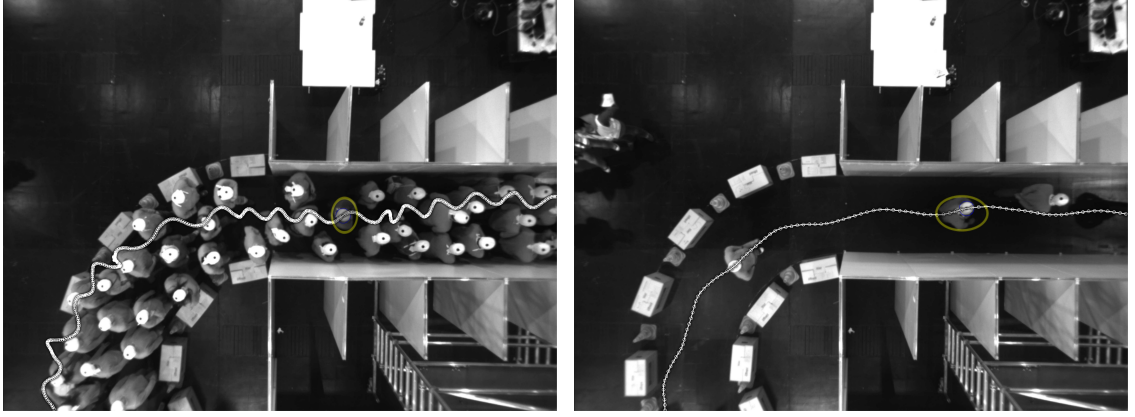
Figure 4.1: Off-line trajectory detection with PeTrack [4]. Left: The trajectory of the detected pedestrian shows strong swaying. Right: The faster pedestrians move, the smoother and weaker is the swaying of their trajectories.

move with their free velocity (Fig. 4.1). Thus we describe with b the lateral swaying of pedestrians and set

$$b = b_{\max} - (b_{\max} - b_{\min})\frac{v_i}{v_i^0} \tag{4.2}$$

Since a and b are velocity-dependent, the inequality

$$b \leq a \tag{4.3}$$

does not always hold for the ellipse i. In the rest of this work we denote the semi-axis in the movement direction by a and its orthogonal semi-axis by b. The definition of the lateral axis in Eq. (4.2) assumes that pedestrians always have an intending speed and do not intend to stay motionless, e.g. waiting for the train in rail-way stations. For those scenarios the model is not convenient and should indeed be generalized.

4.2   Distance between ellipses

In the following we give details for the calculation of the distance d_{ij} between two ellipses which is defined as the distance between the borders of the ellipses, along a

line connecting their centers (Fig. 4.2).

By proper choice of the coordinate system the ellipse i may be written as quadratic form,

$$\frac{x^2}{a_i^2} + \frac{y^2}{b_i^2} = 1 \, . \tag{4.4}$$

In polar coordinates, with the origin at the center of the ellipse and with the angular coordinate α_i measured from the major axis, one gets

$$x = r_i \cos(\alpha_i) \, , \qquad y = r_i \sin(\alpha_i) \, . \tag{4.5}$$

By replacing the expressions of x and y in Eq. (4.4) and rearranging we obtain the expression

$$q r_i^2 - 1 = 0, \tag{4.6}$$

for the polar radius r_i with

$$q = \frac{\cos^2 \alpha_i}{a_i^2} + \frac{\sin^2 \alpha_i}{b_i^2} \, . \tag{4.7}$$

In the same manner we determine the polar radius r_j.

Finally, the distance d_{ij} is determined as follows (Fig. 4.2):

$$d_{ij} = \| \overrightarrow{o_i o_j} \| - r_i - r_j \, . \tag{4.8}$$
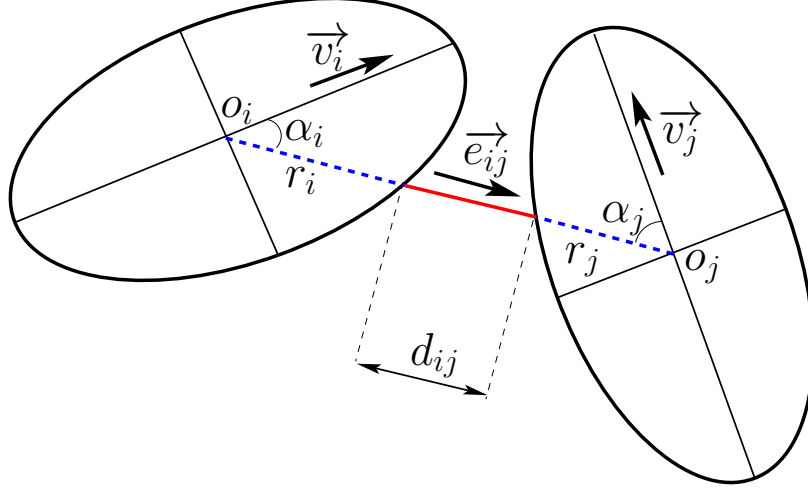
Figure 4.2: d_{ij} is the distance between the borders of the ellipses i and j along a line connecting their centers.

Note that the distance between two ellipses can be non-zero even when the ellipses touch or overlap, see Fig. 4.3. Therefore the forces are generically different from those between circles, even for the same configuration.

4.3 Distance of closest approach

As the repulsive force (3.6) depends inversely on the distance between two pedestrians, it becomes maximal when two pedestrians are in contact. As a consequence of the anisotropy of ellipses the contact distance is in general not zero. In following we give a definition of this distance.

4.3.1 Distance of Closest Approach of two Ellipses

The Distance of Closest Approach (DCA) of two ellipses is the smallest distance between their borders, along a line connecting their centers while they are not overlapping (see Fig. 4.3).

To mitigate overlapping the repulsive forces are high for distances in a certain neighborhood of the distance of closest approach, see $\tilde{l}$ in Fig. 3.4. An analytic

solution of this distance for two arbitrary ellipses is presented in [134]. The main idea of the solution is to transform the ellipse-ellipse problem to a circle-ellipse one, by appropriate transformation.
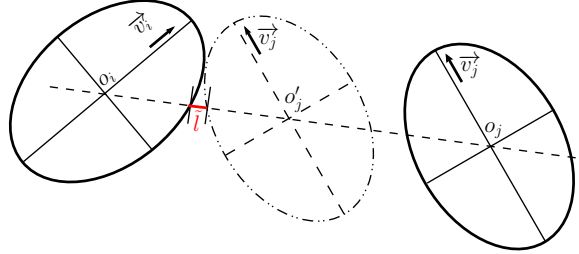
Figure 4.3: Distance of closest approach of two ellipses.

4.3.2 Distance of Closest Approach of an Ellipse to a Line Segment

Similarly to the definition of the distance of closest approach for two arbitrary ellipses [134] we define the DCA for an arbitrary ellipse and a line segment. This distance is needed to calculate the repulsive force between a pedestrian and a wall as defined in Eq. (3.6). See also Fig. 4.4.
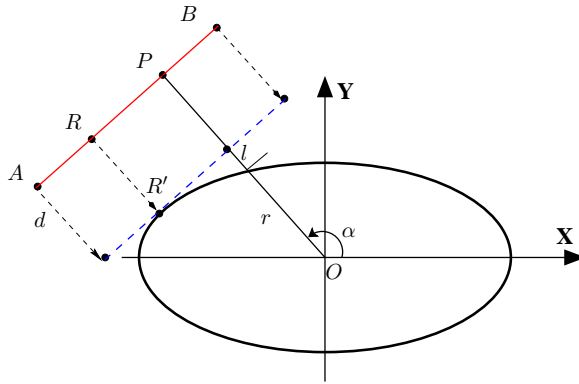
Figure 4.4: Distance of closest approach between an ellipse and a line.

For two points A and B $[AB]$ denotes the line segments delimited with A and B while (AB) denotes the line joining A and B.

Let E be an ellipse with semi-axis a and b and a segment line $[AB]$. We assume without loss of generality that E is in canonical position (center at origin of the coordinate system O and its major and minor semi-axis are parallel to the X-axis and the Y-axis), (Fig. 4.4).

The problem that we want to solve in this section is finding the DCA l of an ellipse E and a line segment $[AB]$.

From Fig. 4.4 bottom one can see that

$$l = \| \overrightarrow{OP} \| - r - d \tag{4.9}$$

P is the nearest point on $[AB]$ to O.

Knowing α we can easily calculate r. To solve Eq. (4.9) one has to find the quantity d, which would be the necessary amount to translate $[AB]$ along the direction of $\overrightarrow{OP}$ such that it becomes tangential to the ellipse.

Let R' be the translation of R in the direction $\overrightarrow{PO}$ by d. Then

$$x_{R'} = x_R - d \cdot \cos(\alpha); \qquad y_{R'} = y_R - d \cdot \sin(\alpha) \tag{4.10}$$

The parametric definition of the line segment $[AB]$ is

$$x = x_A + u \cdot (x_B - x_A); \quad y = y_A + u \cdot (y_B - y_A); \qquad (u \in [0,\ 1]) \tag{4.11}$$

$x_{R'} \in$ ellipse implies

$$\frac{{x'_R}^2}{a^2} + \frac{{y'_R}^2}{b^2} = 1 \tag{4.12}$$

Or,

$$\frac{(x_R - d \cdot \cos(\alpha))^2}{a^2} + \frac{(y_R - d \cdot \sin(\alpha))^2}{b^2} = 1 \tag{4.13}$$

rearranging Eq. (4.13) to make d the subject yields the quadratic equation

$$p \cdot d^2 + q \cdot d + s = 0 \qquad (4.14)$$

with

$$
\begin{aligned}
p &= \frac{\cos(\alpha)^2}{a^2} + \frac{\sin(\alpha)^2}{b^2} > 0 & (4.15) \\
q &= -2 \cdot \left(\frac{x_R \cdot \cos(\alpha)}{a^2} + \frac{y_R \cdot \sin(\alpha)}{b^2} \right) & (4.16) \\
s &= \frac{x_R^2}{a^2} + \frac{y_R^2}{b^2} - 1 & (4.17)
\end{aligned}
$$

If the point R is known then the solution of the problem is

$$d = \frac{-q - \sqrt{\Delta}}{2 \cdot p} \qquad (4.18)$$

with Δ the discriminant of Eq. (4.14):

$$\Delta = q^2 - 4 \cdot p \cdot s \qquad (4.19)$$

As in general R is not known, we rearrange Eq. (4.13) to make u the subject and become

$$p_1 \cdot u^2 + q_1 \cdot u + s_1 = 0 \qquad (4.20)$$

with

$$
\begin{aligned}
p_1 &= \frac{x_{BA}^2}{a^2} + \frac{y_{BA}^2}{b^2} \geq 0 & (4.21) \\
q_1 &= 2 \cdot \left(\frac{x_A - d \cdot \cos(\alpha)}{a^2} \cdot x_{BA} + \frac{y_A - d \cdot \sin(\alpha)}{b^2} \cdot y_{BA} \right) & (4.22) \\
s_1 &= \frac{(x_A - d \cdot \cos(\alpha))^2}{a^2} + \frac{(y_A - d \cdot \sin(\alpha))^2}{b^2} - 1 & (4.23)
\end{aligned}
$$

with the substitutions $x_{BA} = x_B - x_A$ and $y_{BA} = y_B - y_A$.

Since the line (AB) is tangential to the ellipse, Eq. (4.20) has only one solution. Therefore the discriminant is zero:

$$\Delta = q_1^2 - 4 \cdot p_1 \cdot s_1 = 0, \tag{4.24}$$

which leads to

$$q_1{}^2 = 4 \cdot p_1 \cdot s_1 \tag{4.25}$$

Supposing that O, P, A and B are not collinear we solve Eq. (4.25) and get

$$d_{1,2} = \frac{\pm a \cdot b \cdot \sqrt{p_1} - x_{BA} \cdot y_A + y_{BA} \cdot x_A}{y_{BA} \cdot \cos(\alpha) - x_{BA} \cdot \sin(\alpha)} \tag{4.26}$$

and

$$d = \min(|d_1|, |d_2|). \tag{4.27}$$

For the calculated value of d we find u:

$$u = \frac{-q_1}{2 \cdot p_1} \tag{4.28}$$

and check the inequality:

$$0 < u < 1. \tag{4.29}$$

If the inequality (4.29) does not hold or O, P, A and B are collinear then R is an end point of $[AB]$, i.e. A or B. In this case we solve Eq. (4.18) twice for A and B and get d_A and d_B.

Finally the solution is

$$d = \min(|d_A|, |d_B|). \tag{4.30}$$

4.4 Numerical comparison of different representations of the body

In this section we perform different simulations in order to investigate the influence of the shape of simulated pedestrians on the dynamics of pedestrians. The same simulation scenario as in Sec. 2.3 for $N = 180$ pedestrians is considered.

Following shapes were tested:

1. Ellipses with velocity dependent axes (Eq. (4.1)): $a_{\min} = 18\,\mathrm{cm}$ and $\tau_a = 0.43$ and (Eq. (4.2)): $b_{\min} = 20\,\mathrm{cm}$ and $b_{\max} = 25\,\mathrm{cm}$.

2. Circles with velocity dependent radius (Eq. (4.1)): $a_{\min} = 18\,\mathrm{cm}$ and $\tau_a = 0.43$

3. Circles with constant radius: $a_{\min} = 18\,\mathrm{cm}$ and $\tau_a = 0.0$
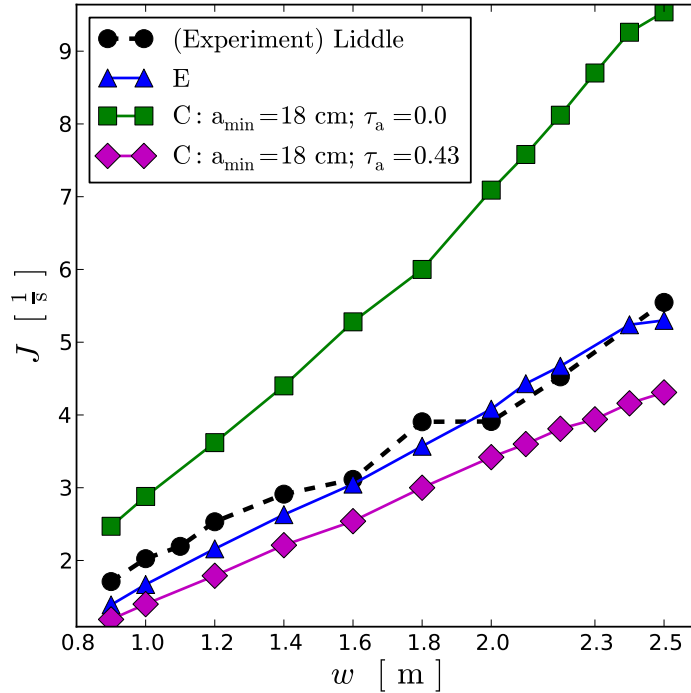
Figure 4.5: Flow in dependence of the width of the bottleneck. Different shapes were simulated and compared. Strategy 2 was used.

By analyzing Fig. 4.5 we asses different conclusions: First, the velocity-dependence of the shape is a key factor in the model. Results of simulation set 3 ($\tau_a = 0$), that corresponds to constant circles, show unrealistically high flow values. Only after making the radius of the circles velocity dependent (simulation set 2) the flow shows values near the empirical range. Second, a direct comparison between ellipses and circles show that in terms of flow values the ellipse results are an upper limit for the circle results. In other words, with the same set of parameter the flow measured with ellipses is higher than the flow measured with circles. Third, we remark that until a width of 1.8 m the flow measured by the simulation set 4 (constant circles with mean radius) is approximately the same as the flow measured by ellipses. For widths bigger that 1.8 m the flow starts to decrease. Those results show, that with constant circles, one can adapt the radius such that the empirical flow still can be satisfactorily reproduced. However, it is difficult to calibrate adequately the radius of the circles for each simulation scenario.

CHAPTER V

Approaches for the desired direction of the driving force

5.1 Introduction

There is a substantial body of literature dealing with the repulsive force and investigating new and better formulation for it. Since the publication of the SFM in 1995 by Helbing [33], several modifications and enhancements were proposed. In [33] the repulsive force was generalized to depend on an equidistant elliptical potential directed in the direction of motion. A slightly different specification of the repulsive force was investigated in [47].

Lakoba et al. [61] mentioned that the original repulsive force exhibits a stiff behavior, thus the equation of motion can not be solved time-efficiently. In order to deal with this problem they proposed a "realistic" modification of the parameters of the repulsive force. The form of the repulsive force and the choice of its parameters was generally discussed in [111] by Steffen and Seyfried. Finally Yu et al. [130] introduced a fully new repulsive force that we generalized in [10].

Somewhat surprisingly, whereas the repulsive force was extensively investigated in the above mentioned works, the influence of the specific form of the driving force (3.4) has so far not attracted much attention.

Although the expression of Eq. (3.4) is simple, it is not clear how to choose the desired direction

$$\overrightarrow{e_i^0} = \frac{\overrightarrow{v_i^0}}{\parallel \overrightarrow{v_i^0} \parallel} \tag{5.1}$$

in a given situation. In most works the direction of (5.1) is neglected. As will be shown later a naive solution like directing pedestrians to a single point leads to artificial jams in particular for wide bottlenecks or corners in large rooms.

In [112] Steffen and Seyfried proposed an Ansatz with directing lines was introduced to steer pedestrians around 90° and 180° corners. In [38] an algorithm for generating automatically a navigation graph in complex buildings in combination with directing lines at corners was proposed. Gloor et al. [21] used a path-oriented approach to model the desired direction of agents with given hiking paths. In [72] the determination of the desired direction was formulated in form of a minimization problem.

It should be mentioned that the *directing problem* we discuss here, i.e. the determination of the desired direction for each pedestrian, is conceptually different from the classical *routing problem.* In [38] an algorithm for generating automatically a navigation graph in complex buildings in combination with directing lines at corners was proposed. Another algorithm for way finding in buildings was proposed in [48]. Recently a further development of the notion of the "quickest path" using a non-iterative method to estimate the desired direction in the SFM was introduced [56]. The main concern in this class of problems is how to define and connect intermediate targets, in order to facilitate the evacuation of pedestrians. By contrast, in the directing problem the existence of such intermediate targets is in general assumed.

59

5.2 Investigating the influence of the desired direction

In this section we show on the basis of the GCFM the impact of the desired direction on the dynamics of a system by measuring the outflow from a bottleneck with different widths. To avoid an abrupt change in the interactions between pedestrians that leaves and those still in the bottleneck, we consider an extension of $e = 2\,\mathrm{m}$ (Fig. 5.1). For the sake of demonstration, four different methods for setting the direction of the desired velocity are suggested. After explaining each strategy a brief qualitative analysis of simulation results is discussed.
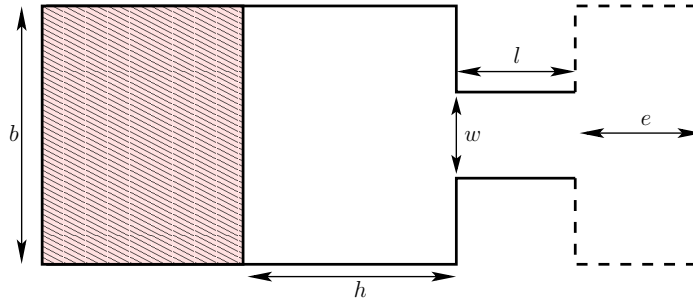
Figure 5.1: Scenario set-up. Pedestrians move from a holding area (shaded area) through the bottleneck ($l = 2.8\,\mathrm{m}$, $h = 4.5\,\mathrm{m}$, $b = 4\,\mathrm{m}$ and w variable). $e = 2\,\mathrm{m}$ is the length of the extra space adjacent to the bottleneck.

All the results shown in this chapter are specific for uni-directional movement. Thus, the impact of the herein presented strategies in bi-directional movement is unclear and should be studied in more details. In this work however, we limit our investigations to the uni-direction case.

5.2.1 Strategy 1: Directing towards the middle of the exit

Maybe the first strategy is the most obvious one. Herein, the choice of the desired direction for a pedestrian i, $\overrightarrow{e_i^0}$, is permanently directed toward a reference point that lies on the middle of the exit. In some situations it happens that pedestrians can not get to the chosen reference point without colliding with walls. To avoid this and to

make sure that all pedestrians can see the middle of the exit the reference point e_1 is shifted by half the minimal shoulder length $b_{\min}$ (Fig. 5.2). Pedestrians that pass to the right of the reference point e_1 head towards e_2.
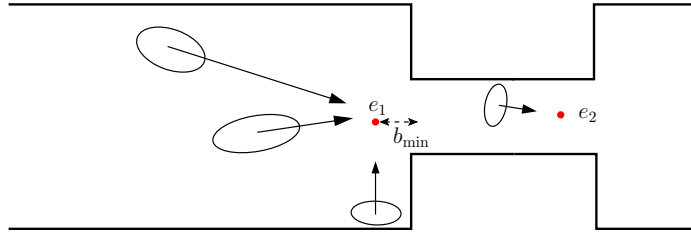
Figure 5.2: Strategy 1. All pedestrians are directed towards the reference points e_1 and e_2.

In Fig. 5.3 we observe that pedestrians are arching in front of the bottleneck. The colors of pedestrians reflect their velocity. The red color (very low velocity) is a sign for jamming. This is explained by the fact, that with this strategy pedestrians are not exploiting the whole width of the bottleneck w and hinder each other. We have $w_{\mathrm{eff}} \ll w$, with w_{eff} the effective with of the bottleneck.

Figure 5.3: Screenshot of a simulation with strategy 1. Top: Width of the bottleneck $w = 1.2\,\mathrm{m}$. Bottom: Width of the bottleneck $w = 2.5\,\mathrm{m}$

5.2.2 Strategy 2: Enhanced directing towards the middle of the exit

This is a modification of strategy 1. Pedestrian are still directed to the shifted reference point e_1. However, from a certain positions pedestrians can see through the bottleneck the second reference point e_2. In this case e_1 is ignored and the desired direction is set to be parallel to the line $\overrightarrow{e_1 e_2}$.

Here again the reference points and the delimiting range of the bottleneck is shifted in $X-$ and $Y-$axis by $b_{\max}$. See Fig 5.4.
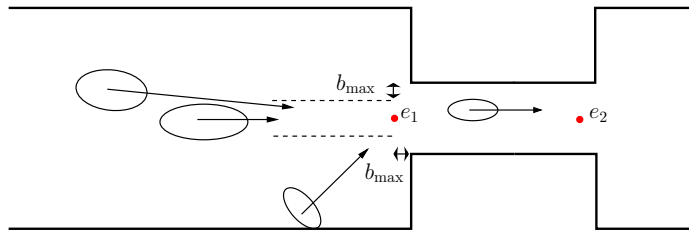
Figure 5.4: Strategy 2. Depending on their position pedestrians adapt their direction. In the range where the exit of the bottleneck is visible (marked with dashed lines) the direction is longitudinal. Outside this area they are directed towards the middle of the bottleneck.

Simulations with strategy 2 (see Fig. 5.5) show, that in contrary to strategy 1 the situation in front of the bottleneck is clearly less dense. Due to the better use of the whole width of the bottleneck, the form of the the form of the congestion is different.
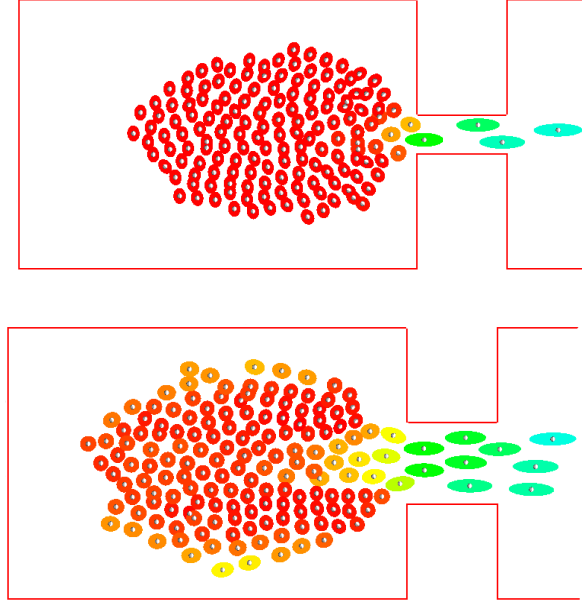
Figure 5.5: Screenshot of a simulation with strategy 2. Top: Width of the bottleneck $w = 1.2\,\text{m}$. Bottom: Width of the bottleneck $w = 2.5\,\text{m}$

5.2.3 Strategy 3: Directing towards the nearest point on the exit

Another possibility to model the desired direction $\overrightarrow{e_i^0}$ is to define a line l in front of the exit and take at each time the nearest point from the pedestrian i to l. In comparison with strategy 2, pedestrians that are not in the range where the point e_2 is not visible choose one of the end points of the line l. In strategy 2 this would be the middle of l (5.6).
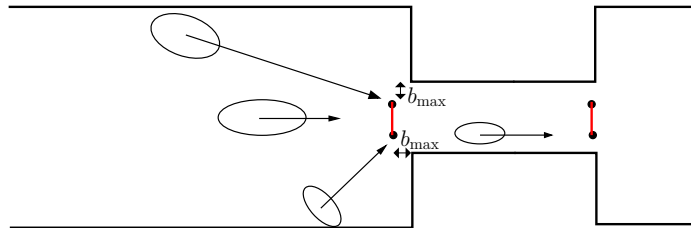
Figure 5.6: Strategy 3. Directing towards the nearest point on the exit. Molnár published in [69] a very similar strategy. The only difference is the placement of the line, which is away from the corner by $b_{\max}$.

In Fig. 5.7 simulations performed with strategy 3 show that like strategy 2 the

use of the whole width of the bottleneck is better than with strategy 1. However, in front of the corners of the bottleneck pedestrians get slightly blocked (red ellipses).
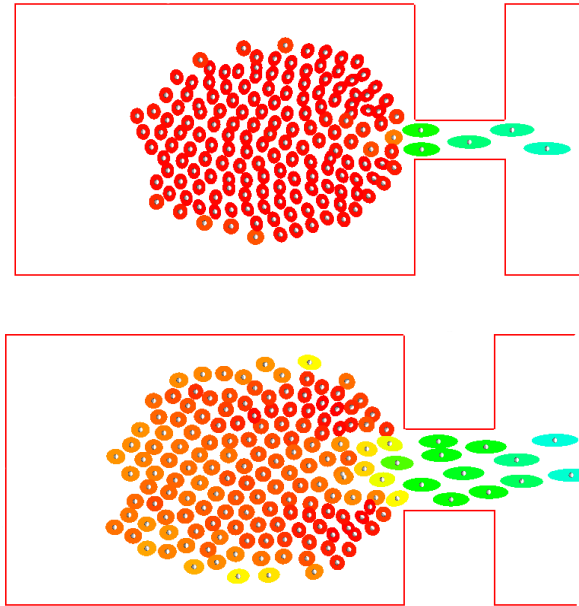
Figure 5.7: Screenshot of a simulation with strategy 3. Top: Width of the bottleneck $w = 1.2\,\mathrm{m}$. Bottom: Width of the bottleneck $w = 2.5\,\mathrm{m}$

The presented strategies are geometry specific. In the next section a more generalized strategy is introduced that can be realized independently on the simulation geometry.

5.3 Guiding line segments for pedestrian orientation in different geometries

All three strategies introduces in the previous section are geometry specific since it is supposed that the exit is always visible to pedestrians. This might not always be the case in all geometries, e.g. corners, T-junctions, etc. In this case one should introduce various "virtual" exits to guide pedestrians from one intermediate target to another.

5.3.1 Introduction strategy 4

Without loss of generality we introduce the main idea of strategy 4 with help of the previous bottleneck. We recall, in strategy 3 a line in front of the bottleneck was defined[1]. The nearest point from each pedestrian to this line was set to define the desired direction. As a generalization we make use in strategy 4 of 3 different lines to "smoothen" merging in front of the bottleneck (Fig 5.8).
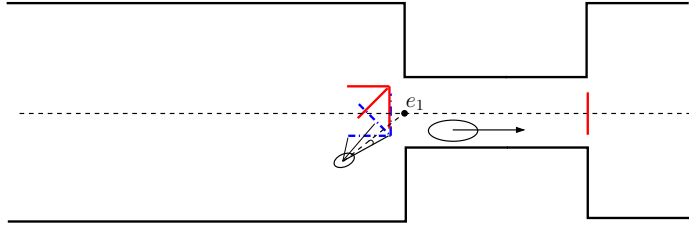
Figure 5.8: Strategy 4. Guiding line segments in front of the bottleneck. For each corner a set of three line segments is generated.

The blue line set (below the dashed line segment) is considered by pedestrians in the lower half of the bottleneck. Respectively, the red line set is considered by pedestrians in the upper half of the bottleneck. Given a pedestrian i at position p_i we define the angle

$$\theta_i = \arccos\left(\frac{\overrightarrow{p_ie_1} \cdot \overrightarrow{p_il_{ij}}}{\parallel \overrightarrow{p_ie_1} \parallel \cdot \parallel \overrightarrow{p_il_{ij}} \parallel}\right),\qquad(5.2)$$

with l_{ij} the nearest point of the line j to the pedestrian i. The next direction is then chosen to be

$$\overrightarrow{e_i^0} = \frac{p_il_{ij}}{\parallel \overrightarrow{p_il_{ij}} \parallel},$$

with j such that $\theta_j = \min\{\theta_1,\ \theta_2\ \theta_3\}$. As in strategy 3 the directing lines are shifted by $b_{\min}$ in in X- and Y-axis.

In Fig. 5.9 simulation results for two different widths are depicted. Simulations were performed with strategy 4. Like strategy 2 and 3 the use of the whole width

---

[1]Some ideas in this section are based on the master thesis of Martina Freialdenhoven: "Modellierung der Wunschrichtung selbstgetriebener Teilchen am Beispiel der Fußgängerdynamik".

of the bottleneck is in comparison to strategy 1 enhanced. The red ellipses show the formation of two lanes of pedestrians that block each other in front of the bottleneck. This is when pedestrians choose from each line set the line that is parallel to the bottleneck.
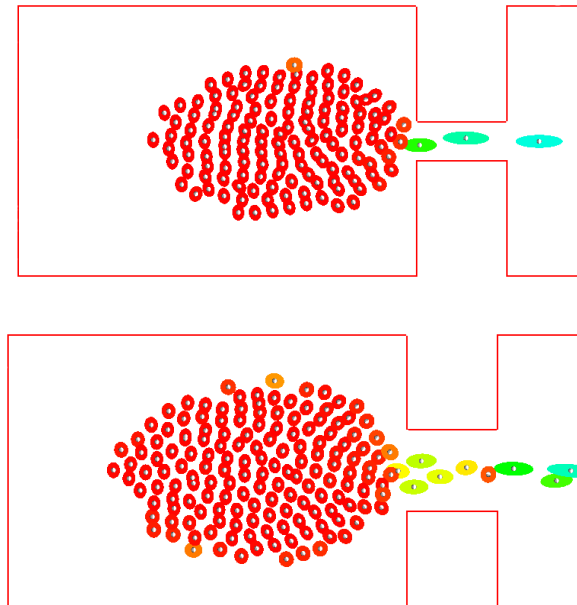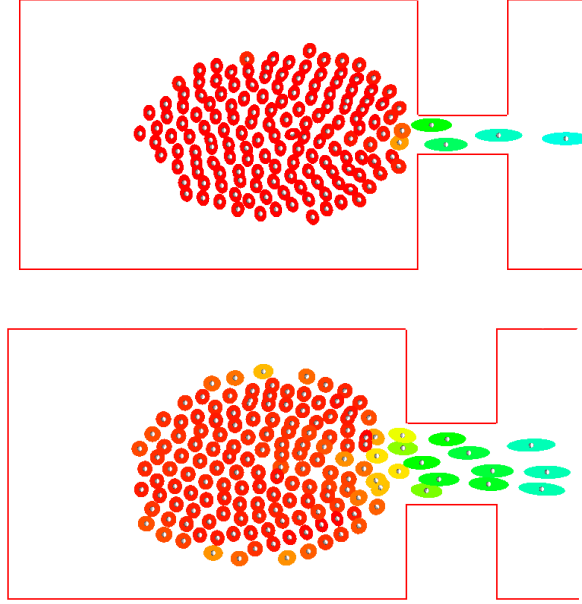

Figure 5.9: Screenshot of a simulation with strategy 4. Top: Width of the bottleneck $w = 1.2\,\text{m}$. Bottom: Width of the bottleneck $w = 2.5\,\text{m}$.

5.3.2 Algorithm to generates guiding line segments

Given two walls, defined by two line segments AB and AC that intersect at the common point A, we define a set of three line segments (Fig. 5.10).

Following, we give the outline of the algorithms to define from each corner the three guiding line segments. First, find the point P on the longer wall such that $\| \overrightarrow{AP} \|$ is equal to the length of the smaller wall (for example AB). The median of the isosceles triangle (BAP) that passes through A intersects BP in the point D. Given a length l the first directing line starts from A is $l_1 = l \cdot \frac{\overrightarrow{DA}}{\|\overrightarrow{DA}\|}$. The two other
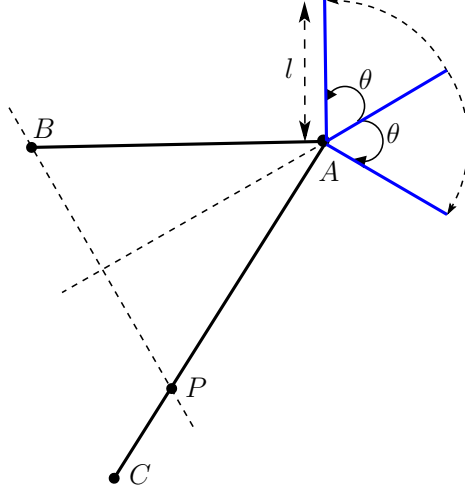
Figure 5.10: Identification of corners by searching for intersecting segment lines (walls). With help of each corner define a set of three guiding line segments. The angle between the guiding line segments is θ and their length is l. θ and l are free parameter that can be adapted conveniently.

lines results from a rotation of l_1 by θ resp. $-\theta$

$$l_2 = M_\theta \cdot l \qquad \& \qquad l_3 = M_{-\theta} \cdot l.$$

With this algorithm it is possible to generate from each intersection of two walls a set of three lines to determine the desired direction. Lines that do not lay inside the geometry should be ignored.

5.3.3 The length of the directing line

So far we used in strategy 4 three different directing lines with length l. One could ask if l should be variable or constant and which length guarantees best results. To study the influence of l on the flow set

$$l = \alpha \cdot w, \tag{5.3}$$

with a constant α. The length of the guiding line depends on the width of the bottleneck. In Fig. 5.11 we show the measurement flow for different values of α.

It becomes clear that longer lines have a negative impact on the flow. This is explained by the fact, that pedestrians are more directed towards the middle of the bottleneck. By short lines, pedestrians tend to be oriented more to regions near the borders of the bottleneck and thus a maximum effective width is used.
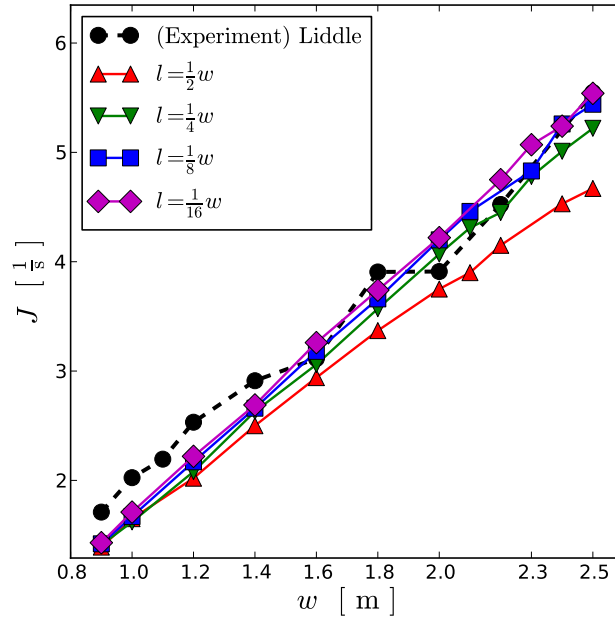
Figure 5.11: Strategy 4: Flow through a bottleneck with different widths and different lengths of the directing lines.

5.3.4 Discussion

In this section we propose different methods (called strategies) how to choose the desired direction $\overrightarrow{e_i^0}$. Simulations results with the GCFM (unchanged set of parameters) of the same bottleneck enables a direct comparison of the used strategy. For each strategy only the width of the bottleneck was varied from $0.9\,\mathrm{m}$ to $2.5\,\mathrm{m}$.

On the basis of a qualitative analysis it was shown how sensitive can be the influence of each strategy on flow. Following we measure for each strategy the flow

from the bottleneck with respect to the width w. The flow is measured directly at the entrance to the bottleneck with the following formula:

$$J = \frac{N_{\Delta t} - 1}{\Delta t},\tag{5.4}$$

with $N_{\Delta t} = 180$ pedestrians and Δt the time necessary that all pedestrians pass the measurement line.

In Fig. 5.12 the resulting flow for all four strategies is presented. The flow measured by strategy 1 stagnates. This was expected since pedestrians do not profit from the whole width of the bottleneck and keep oriented to the middle. The picture changes for strategies 2 – 4, where the effective width of the bottleneck is clearly larger.
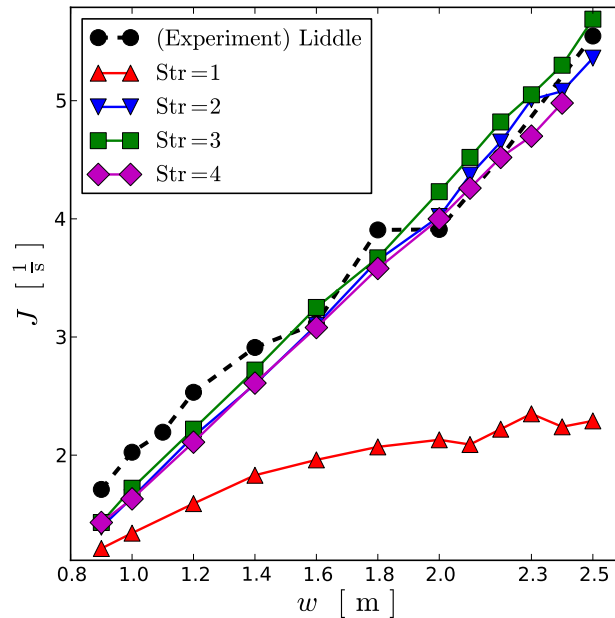
Figure 5.12: Flow through a bottleneck with different widths.

The main observations are:

- The choice of the strategy for the desired direction could influence considerably

the outcome of the simulation.

- A native choice of strategy, in that case strategy 1, can lead to large deviations from experimental results.

- In contrast to strategy 1, strategies 2 – 4 show better usage of the bottleneck width and lead to higher flow values.

5.3.5 Motion around a corner

In this section, we extend strategy 4 and study its impact on the movement time, i.e. the time until all pedestrians have left the simulation set up. For simplicity purposes we consider the movement of $N = 100$ pedestrians in a $90°-$corner-like corridor (Fig. 5.13).
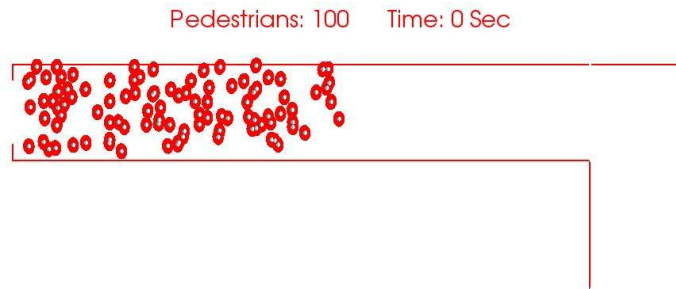
Figure 5.13: Simulation set-up: 100 pedestrians move around the corner with help of guiding lines. Corridor-width is 3 m and its length is 18 m.

The basis of our enhancements is the following observation: Given a guiding line l, the desired direction of a pedestrian i is determined in dependency of its position and the nearest point to l. That means the "choice" of pedestrians neglects two important factors:

1. The geometrical perception of the space: Individuals try when possible to minimize the length of their path to the exit. In our example pedestrian would take a point near the corner as goal and not the nearest point on the guiding line.

This can be, depending on the starting position of pedestrians, far away from the corner and definitely longer that the "shortest path" to the exit.

2. The dynamical and collective influence of pedestrians: In presence of other pedestrians and depending on the magnitude of the local density, the nature of the "quickest path"[2] changes dynamically and differs in most cases from the "shortest path" to the exit.

A similar concept was first introduced in [6] and is well established and widely used in CA. [76, 59]. Burstedde et al. introduced a model based on the notion of static and dynamic floor field that tries to reflect the effects of long-range interactions between the pedestrians. By means of those fields transition rates to neighboring cells are determined. On one hand, the static floor field does not change with time and is geometry specific. It should give a measure of the knowledge of the pedestrians about the geometry. On the other hand, the dynamical floor field is characterized by a virtual trace left by pedestrians. It stimulates the herding behavior of pedestrians. That is e.g. when pedestrian, that are not familiar with the facility just follow others.

At a time step t the nearest point (B_i) to pedestrian i on the guiding line is set to be a first "guess". B_i is uniquely determined by its distance to the end point of the line located next to the edge of the corner A: $l_i(t) = \| \overrightarrow{AB_i} \|$. Since we make use of several guiding lines, we set L_i as the line chosen by pedestrian i.

This distance may be modified at time $t + \Delta t$ depending on two different factors. First factor is static and depends only on the initial $l_i(t)$. Especially it is also independent of the presence of other pedestrians. We define this factor as

$$p_s^i(t) = \exp\left(-\frac{k_s}{l_{\text{rel}}^i(t) + 1}\right), \tag{5.5}$$

<hr>

[2]a term introduced by Kretz et al. in [55].

with

$$l_{\text{rel}}^i(t) = \frac{l^i(t)}{l_{\text{max}}} \tag{5.6}$$

and l_{max} is the width of the guiding line. k_s is a constant that characterizes the tendency of pedestrians to take the shortest path around the corner. $p_s^i(t)$ is reciprocally proportional to the length $l_i(t)$. That means the far away B_i is from A, the larger is $p_s^i(t)$ and thus i tends to change its destination closer to the edge of the corner.

The second factor is of dynamical nature and depends mainly on previous decisions taken by other pedestrians:

$$p_d^i(t) = \exp\left(-k_d \cdot \text{occ}_{\text{rel}}^i(t)\right), \tag{5.7}$$

where

$$\text{occ}_{\text{rel}}^i(t) = \frac{n^i}{n_b^i} \tag{5.8}$$

is a measure of the occupation[3] of the line. n^i is the cardinality of the set

$$A_l = \left\{ l^j \mid j \in B_l \ \& \ l^j < l^i \right\}.$$

That means the number of i's neighbors that are steering towards a point on the segment $[A, B_i]$. n_b^i is the cardinality of the set

$$B_l = \left\{ j \in [1, N] \mid i \neq j \ \& \ L_i \equiv L_j \ \& \ \overrightarrow{e_{i,l}} \cdot \overrightarrow{e_{i,j}} \geq 0 \right\},$$

which is the set of all relevant neighbors of i. By means of a contribution to $\text{occ}_{\text{rel}}^i(t)$ (5.8) they influence i's desired direction. For the scenario depicted in Fig. 5.14 the set B_l for i (red ellipse) contains three pedestrians (bold ellipses), whereas $n^i = 1$ (j). That would give an occupation ratio of $\frac{1}{3}$.

---

[3]not to confound with the *occupation* of a cell in CA-models.

Figure 5.14: How to get around the corner? Pedestrian i that is heading toward the first guiding line, considers the positions of its neighboring pedestrians as well as its initial position to decide whether or not to head closer to the edge of the corner.

Large values of $\mathrm{occ}^i_{\mathrm{rel}}(t)$ imply small values of $p^i_d(t)$. As a consequence pedestrians tend not to change their desired direction closer to the edge of the corner.

Finally, the update rule of the distance $l^i(t)$ is given by

$$l^i(t + \Delta t) = l^i(t) \cdot \Big(1 - \underbrace{p^i_k(t) \cdot p^i_d(t)}_{p^i(t)}\Big). \tag{5.9}$$

$p^i(t) \in [0, 1]$ gives the rate of change from the initial "guess" of pedestrian i. For $p^i(t) = 0$ the desired direction of i stays orthogonal to the guiding line, while $p^i(t) = 1$ displays the case where i's desired direction is direction to the edge of the corner A.

5.3.6 The influence of the sensitivity parameter on the movement time

By means of the sensitivity parameter k_s and k_d it is possible to weight the influence of the above mentioned factors. Fig. 5.15 shows the dynamics observed by changing k_s and k_d.

Figure 5.15: Mean value of the movement time of $N = 100$ pedestrians around a corner in dependency of k_s and k_d. 10 Simulations are performed.

The case $k_s \ll 0$ and $k_d \ll 0$ corresponds to the scenario where all pedestrians try to take the shortest path around the corner. Obviously the short path leads to jams which are reflected by high movement times.

It becomes clear that the behavior of the movement time in dependence of k_s (Fig. 5.15 up) and of k_s (Fig. 5.15 down) is very similar. While the effect of k_d is to change the desire of pedestrian to take the shortest path, the influence of k_s is the following: Initially pedestrians are assumed to target perpendicularly the auxiliary line L and are then motivated, by larger k_s, to move towards the edge of the corner. The question is what if pedestrians directly head toward the edge of the corner? In this case the influence of k_d should be sufficient to drive pedestrians away from the corner and thus reduce the intensity of eventual jams.

By dispensing with the statistical factor $p_s^i(t)$ we simplify the update rule of the distance $l^i(t)$ to

$$l^i(t + \Delta t) = l^i(t) \cdot \left(1 - p_d^i(t)\right). \tag{5.10}$$

Note that pedestrians still show a statistical sense for the geometry by choosing the

inner point of the geometry as a reference point.

5.3.7 Analysis of the sensitivity parameter k_d

To understand the impact of the collective influence of pedestrians on the chosen target point for each pedestrian i, we study the time evolution of the quantities defined in Eqs. (5.8), (5.6) and (5.10) for different values of k_d. The movement of $N = 100$ pedestrians around a corner for different values of k_d is investigated. In order to simplify our tests, only k_d of the first line is varied. Pedestrians steer orthogonally to the second and third line, which corresponds to very high values of k_d.

Fig. 5.16 shows the case $k_d = 0$. The rate of change p is constantly equal to one. That means that the relative distance l_{rel} decreases with time. The occupation ratio is zero for pedestrians that move directly alongside the wall or one for the rest. That is comprehensible since for pedestrian i all relevant pedestrians are also heading towards A, thus $n^i = n^i_{\mathrm{max}}$.
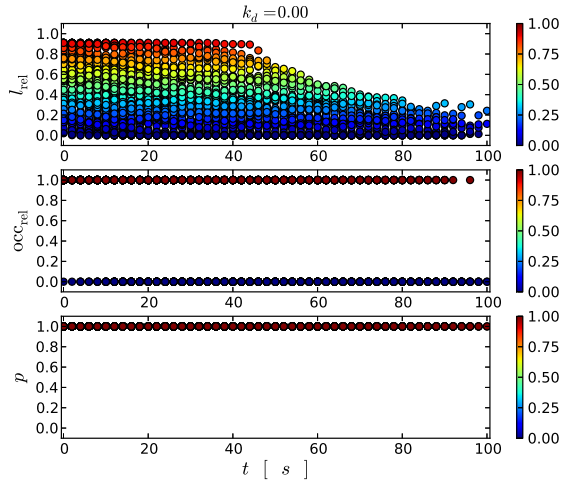
Figure 5.16: $k_d = 0$: The time-evolution of the relative length l_{rel}, the occupation ratio $\mathrm{occ}_{\mathrm{rel}}$ and the rate of change p.

The situation changes considerably when $k_d \neq 0$. Figs. 5.17 and. 5.18 show how the range of spread of p grows from zero to ≈ 0.4 for $k_d = 0.5$ and ≈ 0.6 for $k_d = 1$.

To that effect, the relative occupation $\mathrm{occ_{rel}}$ takes steadily more values in the interval $[0, 1]$. As a consequence, the relative length l_{rel} remains constant for longer time, which indicates that more pedestrians get influenced by others, that are heading towards the corner edge A.
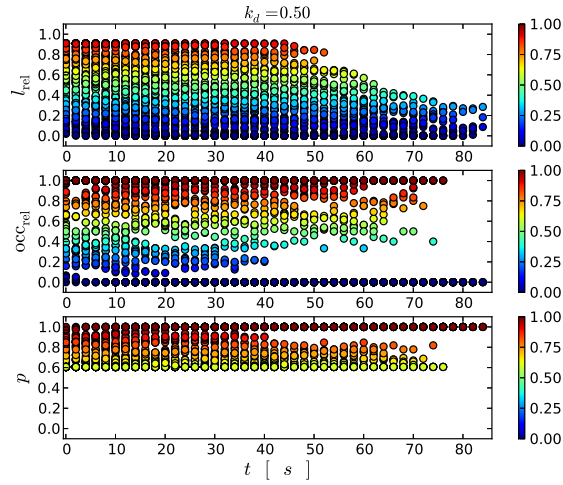
Figure 5.17: $k_d = 0.5$: The time-evolution of the relative length l_{rel}, the occupation ratio $\mathrm{occ_{rel}}$ and the rate of change p.
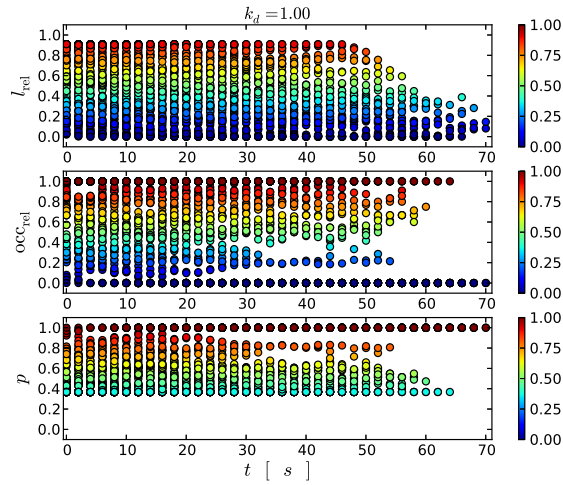
Figure 5.18: $k_d = 1$: The time-evolution of the relative length l_{rel}, the occupation ratio $\mathrm{occ_{rel}}$ and the rate of change p.

Finally, for $k_d = 10$ the collective influence of pedestrians dominates the choice of the desired direction, which is mostly chosen to be orthogonal to the guiding lines. Like the case $k_d = 0$ this is an extreme case that excludes pedestrians willing to take the shortest path around the corner.
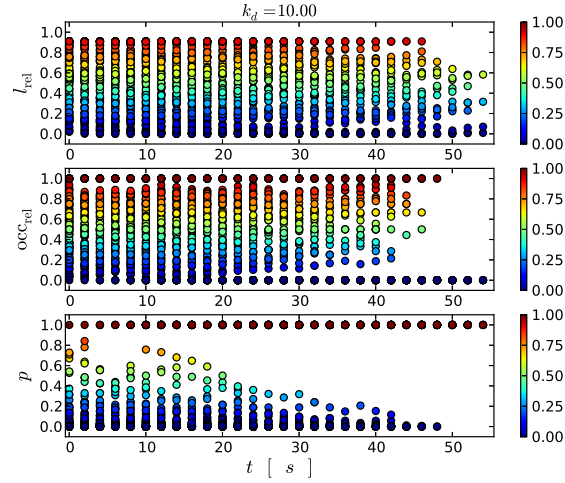
Figure 5.19: $k_d = 10$: The time-evolution of the relative length l_{rel}, the occupation ratio $\mathrm{occ}_{\mathrm{rel}}$ and the rate of change p.

To showcase the impact of the collective influence of pedestrians on evacuation time and jam building, we measure the variation of the movement time in dependence of k_d (Fig. 5.20).
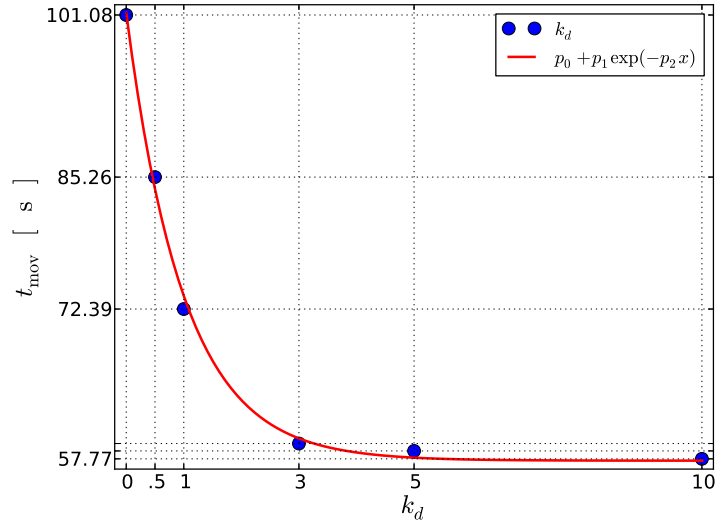
Figure 5.20: Movement time for a simulation with $N = 100$ pedestrians around a corner for different values of k_d. The parameters p_i of the optimal fit (red curve) were calculated with the Levenberg-Marquandt algorithm [70].

We note that the movement time decays exponentially with k_d. For $k_d \geq 3$ there is no relevant change in the dynamics. The qualitative comparison shown in Fig. 5.21 confirms the above-mentioned quantitative analysis.
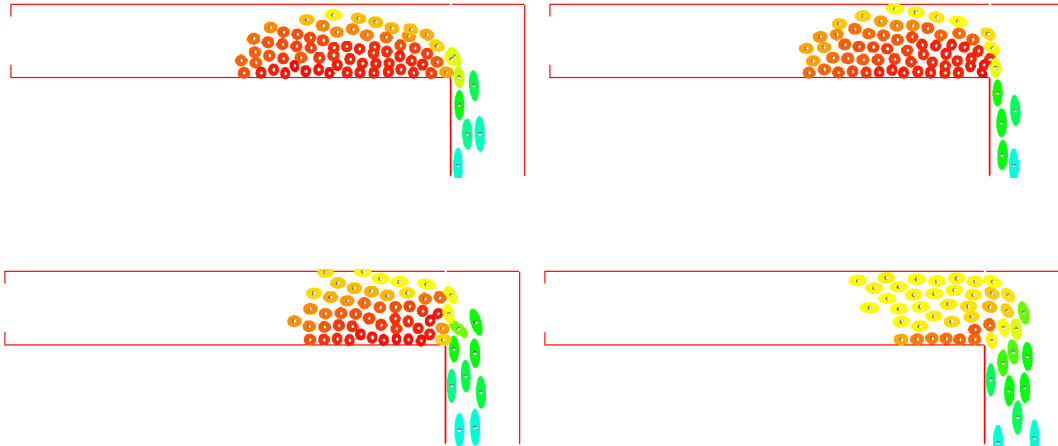
Figure 5.21: Screenshots of simulations with 100 pedestrians. Top left: $k_d = 0$. Top right: $k_d = 0.5$. Bottom left: $k_d = 1$. Bottom right: $k_d = 10$. All screenshots were taken at the same simulation time of $35\,\mathrm{s}$.

For $k_d = 0$ the red ellipses (low velocity) indicate the existence of a jam immediately before the corner. This results from the big competition among the pedestrian to pass through the edge of the corner A. Whereas, for $k_d = 10$ pedestrians move quicker, since they hardly compete for A.

In summary, we presented a strategy to define the desired direction $\overrightarrow{e_i^0}$ for each pedestrian i. This method can be used in general in each geometry characterized by the existence of corners, e.g. Bottlenecks (2 corners), T-junctions (2 corners). In analogy to CA models we introduced and tested two factors to model the statistical and dynamical interaction of pedestrians with the geometry. For a realistic movement around the corner it would be useful to make the value of k_d pedestrian-dependent. That would reflect the heterogeneity of the decision pedestrians make, when choosing between the shortest and quickest path out to the exit.

In contrary to a "commonly believed fact" [56] the desired direction even in elementary geometries is *not* obvious. We showed that the choice of the strategy for the desired direction influences considerably the outcome of the simulation.

CHAPTER VI

Simulations and validation of the GCFM

Computer *simulation* is the mathematical pendant of calculus. It is then essential when equations can not be solved analytically. Its practical significance has been widely acknowledged in the science. Just as observation is extended by experiments, calculation is extended by simulations and are often the only way to understand the dynamical nature of some systems.

Since force-based models represent the time-evolution of pedestrians, by expressing equations of motion, we make use of simulations to solve numerically those equations and gain insights into the target system.

In order to verify the GCFM and evaluate the impact of the elliptical shape of the volume exclusion in comparison with the circular one we measure the FD in two-dimensional space with the same set of parameter as for the one-dimensional FD.

In the one-dimensional case only the space requirement of pedestrians in movement direction, expressed in terms of the semi-axis a, influences the dynamics of the system. Therefore, one can calibrate at the first step the parameter of the axis a, We set $a_{\min}$ and τ_a (Eq. (4.1)). Then we can proceed with calibrating the parameter of the second axis b by means of the 2-D-FD.

Furthermore, we perform simulations in a bottleneck and compare the flow to empirical data. The measurement method for the velocity, the density and the flow
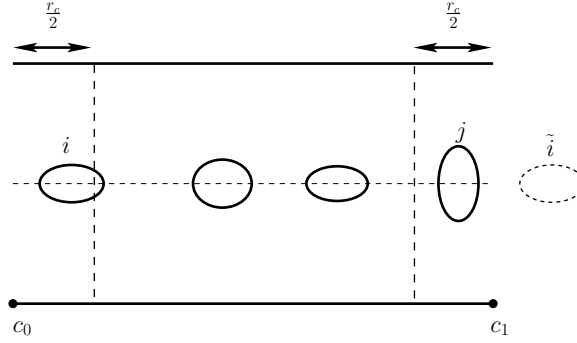
Figure 6.1: One single lane simulation of pedestrian dynamics. To ensure boundary effects, pedestrians moving near the two ends of the corridor interact with each other. In the figure after translating the position of pedestrian i by the length of the corridor, its interaction with pedestrian j is calculated.

are described in App. B.

6.1 One-dimensional fundamental diagram

To illustrate the impact of the velocity-dependence of the radius on the dynamics of pedestrians we measure the FD for 1-D movement in a corridor with periodic boundary conditions. The measurement segment is 2 m long and situated in the middle of the corridor. Details about the measurement method are given in App. B.

The simulation set-up is a straight corridor of 26 m length. The measurement region is 2 m long and situated in the middle of the corridor. In order to reach a large spectrum of densities and to generate stationary data we impose to the system *periodic boundary conditions*. That implies that pedestrians walking near the boundaries of the corridor still interact with each other, as if the extremities of the corridor were connected. Thereby, following conditions should be checked for each two pedestrians i and j:

$$|x_i - c_0| \leq \frac{r_c}{2} \qquad \& \qquad |x_j - c_1| \leq \frac{r_c}{2},$$

with r_c the cut-off of the repulsive force (Fig. 6.1).

Different runs with different number of pedestrians N were performed. To empha-
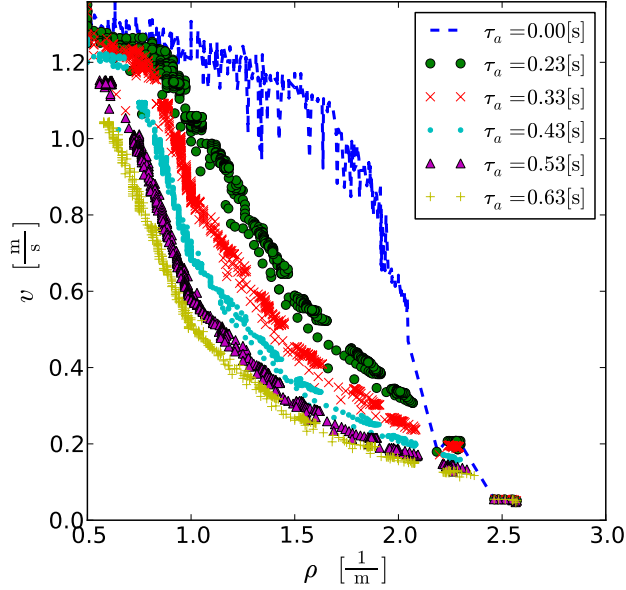
Figure 6.2: Changing τ_a influences the slope of the diagram. $a_{\min}$ has been kept equal to $0.18\,\mathrm{m}$. $\tau_a = 0$ represents pedestrians with constant space-requirement.

size the importance of velocity dependent volume exclusion we vary the parameter τ_a in Eq. (4.1) and measure the FD for each value by keeping the value of $a_{\min}$ constant. In Fig. 6.2 we observe the sensitivity of the FD to the form of the pedestrians. For constant volume exclusion even the curvature of the FD changes. Those findings are in accordance with the results of [106].

Now we verified that both parameters in Eq. (4.1) are necessary and we can not dispense with the velocity-dependence of the radius. The next step would be to find suitable values of the parameters such that the FD match the empirical data. For $\tau_a = 0.53$ s and $a_{\min} = 0.18\,\mathrm{m}$ we can observe a good agreement between simulated and experimental data (Fig. 6.3).
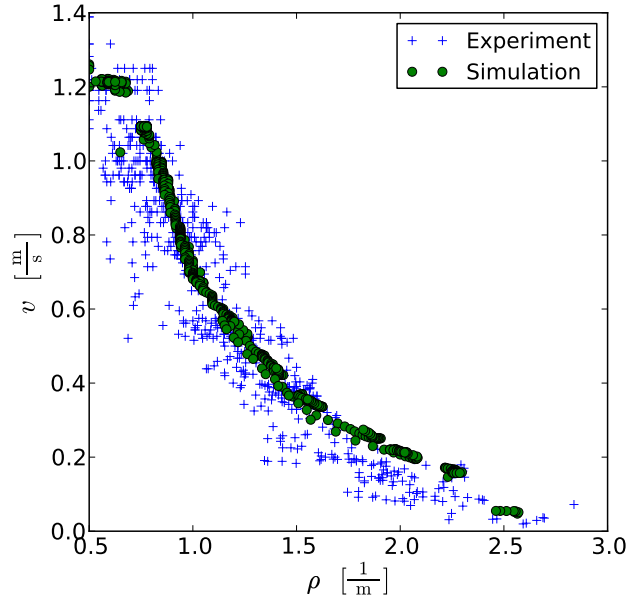
Figure 6.3: Velocity-density relation for one-dimensional movement compared to experimental data [101]. For the simulations, τ_a is set to 0.43 s.

6.2 Two-dimensional fundamental diagram

We extend now the simulation to two-dimensional space and simulate a 25 m $\times$ 1 m corridor with periodic boundary conditions. A measurement segment of 2 m $\times$ 1 m was set in the middle of the corridor. We use the same measurement method as for the single-file case (see App. B). Calibration of the parameters of the lateral semi-axis b ($b_{\min}$ and $b_{\max}$ in Eq. 4.2) leads to the values $b_{\min} = 0.2$ m and $b_{\max} = 0.25$ m. The simulation result is shown in Fig 6.4.

With the chosen dimensions of the semi-axes a and b the model yields the right relation between velocity and density both in single-file movement and wide corridors, although only a corridor width of 1 m was investigated. For the sake of comparison between ellipses and circles, we perform simulations of the same scenario with the same initial values but with circular shaped pedestrians. In Fig. 6.5 the FD is depicted in comparison with experimental data. One remarks that the FD for elliptical
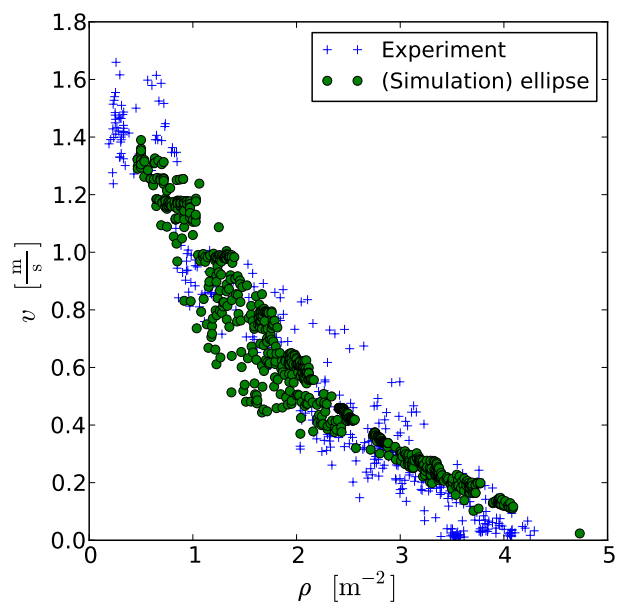
Figure 6.4: Density-velocity relation with *ellipses* in a corridor of dimensions $25 \times 1\,\mathrm{m}^2$ in comparison with experimental data obtained in the HERMES-project [39].
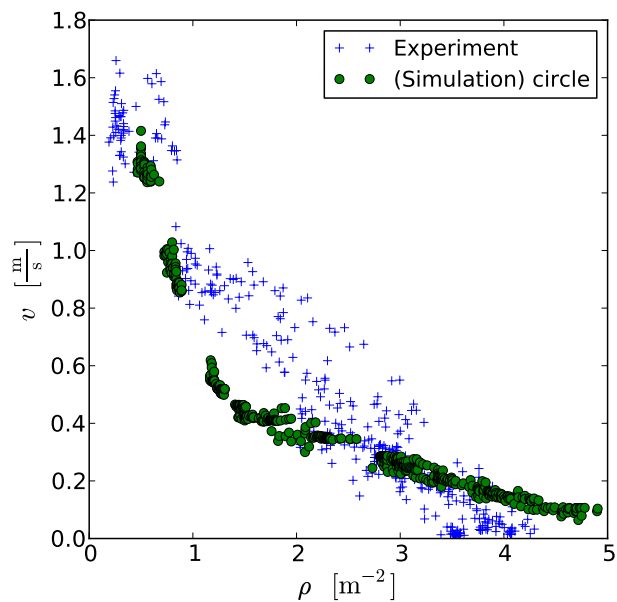
Figure 6.5: Density-velocity relation with *circles* in a corridor of dimensions $25 \times 1\,\mathrm{m}^2$ in comparison with experimental data obtained in the HERMES-project [39]. In these simulations b is set to be equal to a.

shaped pedestrians is an upper bound for that of circular ones, especially at low and medium densities. At high densities with circular pedestrians higher values of velocities are measured. This can be explained with the fact that the chosen shoulder width ($2b_{\min} = 40$ cm) is higher than the minimum space requirement along the movement direction ($a_{\min} = 18$ cm).

In conclusion we can say that ellipses with velocity-dependent semi-axes emulate the space requirement of the projected shape of pedestrians better. Even the shape of the FD is reproduced after inclusion of this velocity-dependence. Finally, the calibrated model yield realistic values of the parameters with physical meaning, e.g. a and b.

6.3 Uni-directional flow in bottlenecks

So far the desired direction in the corridor was parallel to its walls. In other two-dimensional facilities the desired direction changes and becomes, as was shown in Chap. V, crucial to the outcome of the simulation. Therefore, we simulate in this section the outflow from a bottleneck. The simulation set-up is depicted in Fig. 5.1. 180 pedestrian are initially distributed in the holding area. For different widths of the bottleneck we measure the resulting flow. In this simulation we chose strategy 2 to steer pedestrians. Fig. 6.6 shows the results in comparison with experimental data.
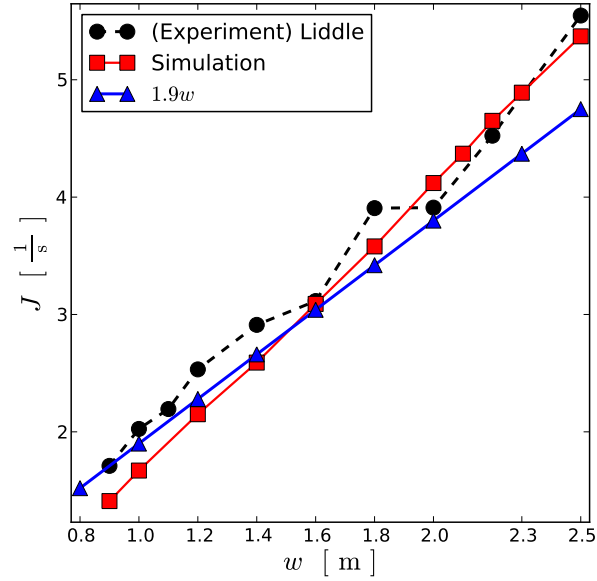
Figure 6.6: The flow in comparison with empirical data from [63].

In summary, the model was systematically validated by considering the dynamics in different geometries. The main challenge hereby is to reproduce the empirical data in various scenarios with *one* set of parameters. Another important aspect is the values that the parameters of the model takes. Especially the parameters that have a physical meaning, e.g. shoulder width (b) and step length (a) should take reasonable values.

This validation process may be continued with simulations in different geometries like T-shaped bottlenecks.

CHAPTER VII

Summary and Outlook

Pedestrian dynamics is a field rich with complex and transient properties that can be addressed by computer simulations. For this purpose several "adjustable-parameter"-models have been already developed. By means of calibration and adjustment of their parameters, they can fit empirical data and are mostly able to describe fairly well observed phenomena, e.g. lane formations.

In principle, before modeling a real-life system, in this case pedestrian dynamics, a decision must be made with regard to the intended purpose of the model and which properties of the system it should cover. For example if the intended purpose of the model is dedicated to visualization issues e.g. pattern recognition, then the designed model should be able to make more or less precise predictions of the trajectories of pedestrians. However for application-orientated purposes a quantitative description of pedestrian dynamics is essential and should be a primary goal of the model.

From a physical point of view, what mostly counts is *understanding* the mechanisms of the underlaying pedestrian's movement. Nevertheless, it should be noticed that an illusion of *understanding* may easily be generated, then the conceived and developed models aim to reproduce qualitatively and quantitatively the collective phenomena that emerges in a dynamical system. To identify and isolate the reasons of such phenomena stays beyond the scope of most mathematical models of pedestrian

dynamics.

In this dissertation modeling of pedestrian dynamics is investigated. A new force-based model is developed and introduced. The minimum description length principle [92] was respected while the conception of the repulsive force. By a proper choice of the force's strength it was possible to find a reasonable compromise between oscillations and overlapping; Two known side-effects of force-based models that are quantified and investigated in this work.

Steering pedestrians by means of the driving force was studied. Especially, in geometries where the visibility of the exit is restricted, considering intermediate goals is necessary. In analogy to the well-known floor-field principle, the desired direction is initialized at each time step in dependence of geometrical as well as dynamical factors that depend on the local dynamics.

The projection of pedestrians on plane is modeled by means of ellipses with velocity-dependent semi-axes. On one side, the semi-axis in the main working direction get larger with increasing speed, which is in accordance with the nature of human walking, i.e. the quicker pedestrians take larger steps and vice versa. On the other side, the semi-axis in shoulder direction shrinks with increasing speed. This feature captures the swaying of the human body while walking.

Finally, the developed model is systematically validated relatively to empirical data. The model contains components that have no influence in some geometries, e.g. the lateral axis in one-dimensional set-ups. This "natural" selection of parameters proved to be beneficial in calibrating only the parameters, that have influence on the simulation in a given scenario. For example, by studying the one dimensional fundamental diagram the parameter of the axis in the movement direction could be adequately calibrated. Considering larger corridors and hence simulating two dimensional unidirectional movement the calibration of the second semi-axis was possible. In corridors the choice of desired direction is trivial, then pedestrians just move for-

wards with minimal detours. This fact will be exploits by simulating bottlenecks and corners, where the desired direction is important in the process of merging. By trying different strategies the dynamics in bottlenecks and the corners was described fairly well.

The proposed model (GCFM) was successfully used in the project Hermes[1], which goal is the development of an evacuation assistant for mass events. The use of different optimization techniques have enabled a real time simulation.

---

[1]Hermes is funded by the German Government (Federal Ministry of Education and Research)

APPENDICES

APPENDIX A

Parameter set for the simulations

For all simulation in this work the initial value problem in Eq. (1.1) was solved using an Euler scheme with fixed-step size $\Delta t = 0.01$ s. First the state variables of all pedestrians are determined. Then the update to the next step is performed. Thus, the update in each step is parallel.

The desired speeds of pedestrians are Gaussian distributed with mean $\mu = 1.34$ m/s and standard deviation $\sigma = 0.26$ m/s. The time constant τ in the driving force Eq. (3.4) is set to 0.5 s, i.e. $\tau \gg \Delta t$. For simplicity, the mass m_i is set to unity. In Tab. A.1 we give an overview about the parameter incorporated in the GCFM.

Parameter	Eq. number	Value
η	(3.6)	0.2
r_c	(3.13)	2 m
$f_{\max}$ (ped-ped)	(3.14)	3
$f_{\max}$ (ped-wall)	(3.14)	10
r_{eps}	(3.15)	0.1 m
τ_a	(4.1)	0.43 s
$a_{\min}$	(4.1)	0.18 m
$b_{\max}$	(4.2)	0.25 m
$b_{\min}$	(4.2)	0.2 m

Table A.1: Parameter values used in simulations if it is not mentioned explicitly that changes have been mad.

91

APPENDIX B

Measurement method

The mean velocity of pedestrian i that enters the measurement are in $(x_i^{\text{in}}, y_i^{\text{in}})$ and leaves it in $(x_i^{\text{out}}, y_i^{\text{out}})$ is determined as

$$v_i = \frac{\sqrt{(x_i^{\text{out}} - x_i^{\text{in}})^2 + (y_i^{\text{out}} - y_i^{\text{in}})^2}}{t_i^{\text{out}} - t_i^{\text{in}}} \tag{B.1}$$

where t_i^{in} is the entrance time and t_i^{out} exit time of i (Fig. B.1).
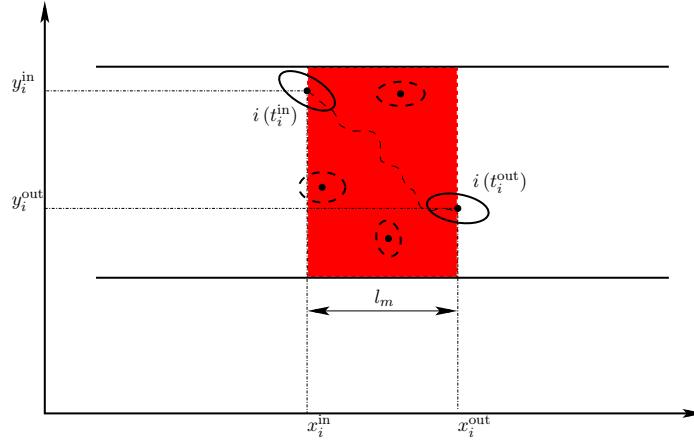
Figure B.1: Pedestrian i enters the measurement area (red) at t_i^{in} in $(x_i^{\text{in}}, y_i^{\text{in}})$ and leaves it at t_i^{out} in $(x_i^{\text{out}}, y_i^{\text{out}})$. The direction of motion is from left to right.

For the one-dimensional case $y_i^{\text{in}} = y_i^{\text{out}} = 0$.

92

The density is defined as follows:

$$\rho_i = \frac{1}{t_i^{\text{out}} - t_i^{\text{in}}} \int_{t_{\text{in}}}^{t_{\text{out}}} \rho(t)\, dt \qquad \text{(B.2)}$$

$$\rho(t) = \frac{N_{\text{in}}(t)}{l_m}. \qquad \text{(B.3)}$$

with $l_m = 2m$ the length of the measurement area in the movement direction and $N_{\text{in}}(t)$ is the number of pedestrians within the area at time t. In one dimensional space the measurement area is reduced to a measurement segment of length l_m.

APPENDIX C

Approximation of the area of an ellipse

In this appendix we give details about the used method to approximate the area of an arbitrary ellipse by means of a polygon. Without loss of generality we consider an ellipse $(\mathcal{E})$ centered at the origin of the coordinate system $\mathcal{S}$ and whose major and minor axes coincide with the axes of $\mathcal{S}$. The points $P_i(x_i, y_i)$, $i = 0, \cdots, n-1$, with

$$
\begin{cases}
x_i = a \cos(i\dfrac{2\pi}{n}) & \text{(C.1)} \\[2mm]
y_i = b \sin(i\dfrac{2\pi}{n}) & \text{(C.2)}
\end{cases}
$$

define a n-sided polygon inscribed in $\mathcal{E}$ (Fig. C.1).
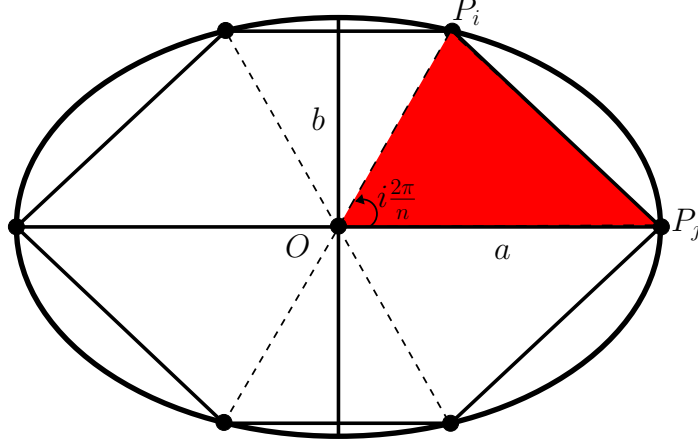
Figure C.1: A 6-sided polygon inscribed in an ellipse. The area of the ellipse can be approximated by the area of the polygon, which is given by the sum of the adjacent triangles $\triangle(OP_iP_j)$, $i = 0, \cdots, n-1, j = (i+1) \mod n$.

The area of the triangle $\mathcal{T}_i = \triangle(OP_iP_j)$ with $j = (i+1) \mod n$, is

$$A_i = \frac{1}{2}|x_iy_j - x_jy_i|. \tag{C.3}$$

Considering the expressions in Eqs. (C.1) and (C.2) we get

$$A_i = \frac{ab}{2}\sin(\frac{2\pi}{n}). \tag{C.4}$$

By summing the areas A_i of the n adjacent triangles $\mathcal{T}_i$ one obtains the area of the polygon as

$$A_n = \sum_{i=0}^{n-1} A_i \tag{C.5}$$

$$= \frac{ab}{2}n\sin(\frac{2\pi}{n}). \tag{C.6}$$

Obviously the area of the ellipse $\mathcal{E}$ is given by A_∞, since

$$A_{n \to \infty} \quad \to \quad \frac{ab}{2} 2\pi \underbrace{\frac{n}{2\pi} \sin(\frac{2\pi}{n})}_{\to 1} \tag{C.7}$$

$$= \quad \pi ab. \tag{C.8}$$

The relative error between the approximated value of the area (A_n) and the exact one (A_∞) is given by

$$\delta = \left| \frac{A_\infty - A_n}{A_\infty} \right|. \tag{C.9}$$

Substituting A_n and A_∞ from Eqs. (C.6) and (C.8) in Eq. (C.9) we get

$$\delta \quad = \quad \left| \frac{\pi ab - ab\frac{n}{2}\sin(\frac{2\pi}{n})}{\pi ab} \right| \tag{C.10}$$

$$= \quad \left| \frac{\pi - \frac{n}{2}\sin(\frac{2\pi}{n})}{\pi} \right|. \tag{C.11}$$

Fig. C.2 depicts the evolution of δ in dependence of the number of vertices. For $n = 40$ we can approximate the area of the ellipse $\mathcal{E}$ with a relative error of $\delta = 0.41 \cdot 10^{-2}$, which is a sufficiently acceptable error in approximating the overlapping ratio (3.21).
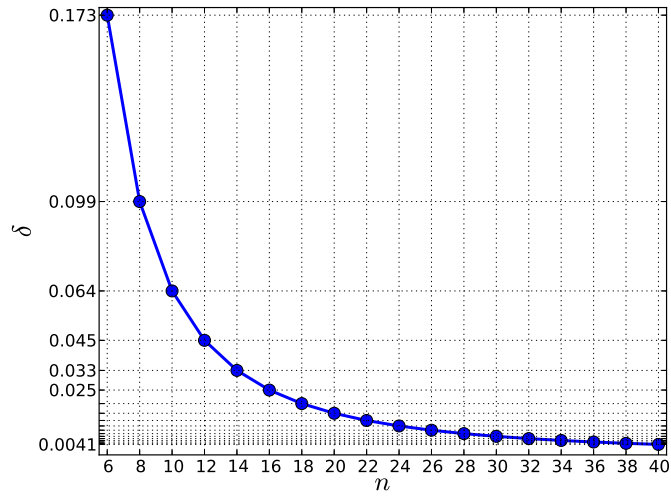
Figure C.2: The relative error of the approximate area of the ellipse by a n-sided inscribed polygon.

The area (C.6) corresponds to the *maximum n*-sided polygon which can be inscribed in an ellipse [83]. Since we are interested in the approximated area, this influences positively the relative error δ.

APPENDIX D

Publications during PhD work

- U. Kemloh, **M. Chraibi**, A. Seyfried, A. Schadschneider. Efficient and validated simulation of crowds for an evacuation assistant. *Comp. Anim. Virtual Worlds*, 2012, vol. 23, pp. $3 - 15$.

- G. B. Hughes and **M. Chraibi**. Calculating ellipse overlap areas. *ArXiv e-prints 1106.3787*, 2011.

- **M. Chraibi**, U. Kemloh, A. Schadschneider, A. Seyfried. Force-based models of pedestrian dynamics. *Networks and Heterogeneous Media*, 2010, vol. 6(3), pp. $425 - 442$.

- **M. Chraibi**, A. Seyfried and A. Schadschneider. Generalized centrifugal force model for pedestrian dynamics, *Phys. Rev. E*, 2010, vol. 82, p. 046111.

- A. Seyfried, **M. Chraibi**, U. Kemloh, J. Mehlich and A. Schadschneider. Run-time Optimization of Forced Based Models within the Hermes Project. *Pedestrian and Evacuation Dynamics*, eds. R.D. Peacock, E.D. Kuligowski, J.D. Averill, pp. $363 - 373$, Springer, 2011

- A. Seyfried, J. Mehlich and **M. Chraibi**. Hermes: An Evacuation Assistant for Mass Events in Complex Buildings − Simulation of Crowd Movement Faster than Realtime. *Proceedings of 2009 first international conference on evacuation modeling and Management*, 23−25 September 2009, in Delft, Neederlands.

- **M. Chraibi**, A. Seyfried, A. Schadschneider and W. Mackens. Quantitative Description of Pedestrian Dynamics with a Force-based Model. *Proceedings of 2009 IEEE/WIC/ACM International Joint Conferences on Web Intelligence and Intelligent Agent Technologies*, 15−18 September 2009, in Milano, Italy.

- **M. Chraibi**, A. Seyfried, A. Schadschneider and W. Mackens. Modifications of the Centrifugal Force Model for Pedestrian Dynamics. *Proceedings of The Conference on Traffic and Granular Flow 2009*, June 22-24 2009

BIBLIOGRAPHY

BIBLIOGRAPHY

[1] *Stairways and Ergonomics*, IL, USA, 2006. ASSE. Proceedings of American Society of Safety Engineers Annual Professional Development Conference, Seattle, 2006.

[2] M. Asano, T. Iryo, and M. Kuwahara. Microscopic pedestrian simulation model combined with a tactical model for route choice behaviour. *Transport Res. C–Emer.*, 18(6):842–855, 2010.

[3] V. J. Blue and J. L. Adler. Cellular automata microsimulation for modeling bidirectional pedestrian walkways. *Transport Res. B–Meth.*, 35(3):293–312, 2001.

[4] M. Boltes, A. Seyfried, B. Steffen, and A. Schadschneider. Using stereo recordings to extract pedestrian trajectories automatically in space. In R. D. Peacock, E. D. Kuligowski, and J. D. Averill, editors, *Pedestrian and Evacuation Dynamics*, pages 751–754, US, 2010. Springer.

[5] S. Burghardt, A. Seyfried, and W. Klingsch. Improving egress design through measurement and correct interpretation of the fundamental diagram for stairs. In M. Panda and U. Chattaraj, editors, *Developments in Road Transportation*, pages 181–187. Macmillan Publishers India Ltd, 2010.

[6] C. Burstedde, K. Klauck, A. Schadschneider, and J. Zittartz. Simulation of pedestrian dynamics using a two-dimensional cellular automaton. *Physica A*, 295(3–4):507–525, 2001.

[7] U. Chattaraj, A. Seyfried, and P. Chakroborty. Comparison of pedestrian fundamental diagram across cultures. *Advances in Complex Systems*, 12(3):393–405, 2009.

[8] D. Chowdhury, L. Santen, and A. Schadschneider. Statistical physics of vehicular traffic and some related systems. *Phy. Rep.*, 329(4–6):199–329, 2000.

[9] M. Chraibi and A. Seyfried. Pedestrian dynamics with event-driven simulation. In W. W. F. Klingsch, C. Rogsch, A. Schadschneider, and M. Schreckenberg, editors, *Pedestrian and Evacuation Dynamics 2008*, pages 713–718, Berlin Heidelberg, 2010. Springer.

[10] M. Chraibi, A. Seyfried, and A. Schadschneider. The generalized centrifugal force model for pedestrian dynamics. *Phys. Rev. E*, 82:046111, 2010.

[11] M. Chraibi, A. Seyfried, A. Schadschneider, and W. Mackens. Quantitative description of pedestrian dynamics with a force-based model. In *IEEE/WIC/ACM International Joint Conference on Web Intelligence and Intelligent Agent Technology*, volume 3, pages 583–586. IEEE Computer Society, 2009.

[12] S. Curtis, J. Stephen, B. Zafar, and D. Manocha. Virtual tawaf: A case study in simulating the behavior of dense, heterogeneous crowds. In *IEEE Workshop on Modeling, Simulation and Visual Analysis of Large Crowds*, pages 128–135. IEEE, 2011.

[13] W. Daamen, P. Bovy, and S. Hoogendoorn. Modelling pedestrians in transfer stations. In M. Schreckenberg and S. D. Scharma, editors, *Pedestrian and Evacuation Dynamics*, pages 59–73. Springer, 2002.

[14] W. Daamen and S. Hoogendoorn. First international conference on evacuation modeling and management capacity of doors during evacuation conditions. *Procedia Engineering*, 3:53–66, 2010.

[15] M. Davidich and G. Köster. Towards automatic and robust adjustment of human behavioral parameters in a pedestrian stream model to measured data. In R. D. Peacock, E. D. Kuligowski, and J. D. Averill, editors, *Pedestrian and Evacuation Dynamics 2010*, pages 535–536, US, 2010. Springer.

[16] M. Davidich and G. Köster. Towards automatic and robust adjustment of human behavioral parameters in a pedestrian stream model to measured data. *Safety Sci.*, 50(5):1253–1260, 2012.

[17] Z. Fang, J. P. Yuan, Y. C. Wang, and S. M. Lo. Survey of pedestrian movement and development of a crowd dynamics model. *Fire Safety J.*, 43(6):459–465, 2008.

[18] J. J. Fruin. *Pedestrian Planning and Design*. Elevator World, New York, 1971.

[19] P. G. Gipps. Simulation of Pedestrian Traffic in Buildings. Technical Report 35, Institut für Verkehrswesen Universität (TH) Karlsruhe, 1986.

[20] P. G. Gipps and B. Marksjö. A micro-simulation model for pedestrian flows. *Math. Comput. Simulat.*, 27(2–3):95–105, 1985.

[21] C. Gloor, L. Mauron, and K. Nagel. A pedestrian simulation for hiking in the alps. In *Swiss Transport Research Conference*, Monte Verita, 2003.

[22] B. D. Hankin and R. A. Wright. Passenger flow in subways. *Oper. Res. Soc.*, 9(2):81–88, 1958.

[23] D. Hartmann. Adaptive pedestrian dynamics based on geodesics. *New Journal of Physics*, 12:043032, 2010.

[24] D. Helbing. A mathematical model for the behavior of pedestrians. *Behav. Sci.*, 36(4):298–310, 1991.

[25] D. Helbing. A fluid dynamic model for the movement of pedestrians. *Complex Systems*, 6:391–415, 1992.

[26] D. Helbing. Collective phenomena and states in traffic and self-driven many-particle systems. *Comp. Mater. Sci.*, 30(1–2):180–187, 2004.

[27] D. Helbing, L. Buzna, A. Johansson, and T. Werner. Self-organized pedestrian crowd dynamics: Experiments, simulations, and design solutions. *Transport. Sci.*, 39(1):1–24, 2005.

[28] D. Helbing, I. Farkas, and T. Vicsek. Simulating dynamical features of escape panic. *Nature*, 407:487–490, 2000.

[29] D. Helbing, I. J. Farkas, P. Molnár, and T. Vicsek. Simulation of pedestrian crowds in normal and evacuation situations. In M. Schreckenberg and S. D. Scharma, editors, *Pedestrian and Evacuation Dynamics*, pages 21–58. Springer, 2002.

[30] D. Helbing, I. J. Farkas, and T. Vicsek. Freezing by heating in a driven mesoscopic system. *Phys. Rev. Let.*, 84:1240–1243, 2000.

[31] D. Helbing, R. Jiang, and M. Treiber. Analytical investigation of oscillations in intersecting flows of pedestrian and vehicle traffic. *Phys. Rev. E*, 72:046130, 2005.

[32] D. Helbing, A. Johansson, and H. Z. Al-Abideen. Dynamics of crowd disasters: An empirical study. *Phys. Rev. E*, 75:046109, 2007.

[33] D. Helbing and P. Molnár. Social force model for pedestrian dynamics. *Phys. Rev. E*, 51:4282–4286, 1995.

[34] L. F. Henderson. The statistics of crowd fluids. *Nature*, 229(05):381–383, 1971.

[35] L. F. Henderson. On the fluid mechanics of human crowd motion. *Transport. Res.*, 8(6):509–515, 1974.

[36] G. T. Herman. Computing ability of a developmental model for filamentous organisms. *J. Theor. Biol.*, 25(3):421–435, 1976.

[37] K. Hirai and K. Tirui. A simulation of the behavior of a crowd in panic. *Systems and Control*, 21(6):331, 1977.

[38] M. Höcker, V. Berkhahn, A. Kneidl, A. Borrmann, and W. Klein. Graph-based approaches for simulating pedestrian dynamics in building models. In *8th European Conference on Product & Process Modelling*, University College Cork, Ireland, 2010.

[39] S. Holl and A. Seyfried. Hermes - an evacuation assistant for mass events. *inSiDe*, 7(1):60–61, 2009.

[40] S. Hoogendoorn and W. Daamen. A novel calibration approach of microscopic pedestrian models. In H. Timmermans, editor, *Pedestrian Behavior: Models, Data Collection and Applications*, page 195. Emerald, 2009.

[41] S. P. Hoogendoorn and W. Daamen. Pedestrian behavior at bottlenecks. *Transport. Sci.*, 39(2):147–159, 2005.

[42] S. P. Hoogendoorn and W. Daamen. Self-organization in pedestrian flow. In S. P. Hoogendoorn, S. Luding, P. H. L. Bovy, M. Schreckenberg, and D. E. Wolf, editors, *Traffic and Granular Flow '03*, pages 373–382. Springer, 2005.

[43] S. P. Hoogendoorn, W. Daamen, and P. H. L. Bovy. Extracting microscopic pedestrian characteristics from video data. In *TRB 2004 Annual Meeting*. Washington DC: National Academy Press, 2003.

[44] S. P. Hoogendoorn, W. Daamen, and R. Landman. Microscopic calibration and validation of pedestrian models - cross-comparison of models using experimental data. In N. Waldau, P. Gattermann, H. Knoflacher, and M. Schreckenberg, editors, *Pedestrian and Evacuation Dynamics 2005*, page 253. Springer, 2007.

[45] G. B. Hughes and M. Chraibi. Calculating ellipse overlap areas. *ArXiv e-prints*, 2011, 1106.3787.

[46] A. Jelić, C. Appert-Rolland, S. Lemercier, and J. Pettré. Properties of pedestrians walking in line – fundamental diagrams. *ArXiv e-prints*, 2011, 1111.5708.

[47] A. Johansson, D. Helbing, and P. K. Shukla. Specification of the social force pedestrian model by evolutionary adjustment to video tracking Data. *Advances in Complex Systems*, 10(2):271–288, 2007.

[48] A. U. Kemloh Wagoum and A. Seyfried. Optimizing the evacuation time of pedestrians in a graph-based navigation. In M. Panda and U. Chattararaj, editors, *Developments in Road Transportation*, pages 188–196. Macmillan Publishers India Ltd, 2010.

[49] A. Kirchner. *Modellierung und statistische Physik biologischer und sozialer Systeme*. Dissertation, Universität zu Köln, 2003.

[50] A. Kirchner, K. Nishinari, and A. Schadschneider. Friction effects and clogging in a cellular automaton model for pedestrian dynamics. *Phys. Rev. E*, 67:056122, 2003.

[51] A. Kirchner and A. Schadschneider. Simulation of evacuation processes using a bionics-inspired cellular automaton model for pedestrian dynamics. *Physica A*, 312:260–276, 2002.

[52] W. Klein, G. Köster, and A. Meister. Towards the calibration of pedestrian stream models. In R. Wyrzykowski, J. Dongarra, K. Karczewski, and J. Wasniewski, editors, *Proceedings of the 8th international conference on Parallel processing and applied mathematics: Part II*, PPAM'09, pages 521–528, Berlin Heidelberg, 2010. Springer.

[53] T. Korhonen, S. Hostikka, and O. Keski-Rahkonen. A proposal for the goals and new techniques of modelling pedestrian evacuation in fires. *Fire Safety Science*, 7:557–567, 2005.

[54] G. Köster, D. Hartmann, and W. Klein. Microscopic pedestrian simulations: From passenger exchange times to regional evacuation. In B. Hu, K. Morasch, M. Siegle, and S. Pickl, editors, *Operations Research Proceedings 2010*. Springer, 2011.

[55] T. Kretz. Pedestrian traffic: on the quickest path. *J. Stat. Mech.–Theory E.*, P03012, 2009.

[56] T. Kretz, A. Große, S. Hengst, L. Kautzsch, A. Pohlmann, and P. Vortisch. Quickest paths in simulations of pedestrians. *Advances in Complex Systems*, 14(5):733–759, 2011, 1107.2004.

[57] T. Kretz, A. Grünebohm, and M. Schreckenberg. Experimental study of pedestrian flow through a bottleneck. *J. Stat. Mech.–Theory E.*, 2006(10):P10014, 2006, physics/0610077.

[58] T. Kretz, S. Hengst, and P. Vortisch. Pedestrian flow at bottlenecks - validation and calibration of vissim's social force model of pedestrian traffic and its empirical foundations. In M. Sarvi, editor, *International Symposium of Transport Simulation 2008*, page electronic publication, Gold Coast, Australia, 2008. Monash University, 0805.1788.

[59] T. Kretz and M. Schreckenberg. The F.A.S.T.-Model. In S. El Yacoubi, B. Chopard, and S. Bandini, editors, *Cellular Automata – 7th International Conference on Cellular Automata for Research and Industry, ACRI 2006, Proceedings*, volume 4173/2006 of *Lecture Notes in Computer Science*, pages 712–715, Berlin Heidelberg, 2006. Springer, 0804.1893.

[60] T. Kretz, M. Wölki, and M. Schreckenberg. Characterizing correlations of flow oscillations at bottlenecks. *J. Stat. Mech.–Theory E.*, P02005, 2006, cond-mat/0601021.

[61] T. I. Lakoba, D. J. Kaup, and N. M. Finkelstein. Modifications of the Helbing-Molnár-Farkas-Vicsek social force model for pedestrian evolution. *Simulation*, 81(5):339–352, 2005.

[62] P. Langston, R. Masling, and B. Asmar. Crowd dynamics discrete element multi-circle model. *Safety Science*, 44:395–417, 2006.

[63] J. Liddle, A. Seyfried, W. Klingsch, T. Rupprecht, A. Schadschneider, and A. Winkens. An experimental study of pedestrian congestions: Influence of bottleneck width and length. *ArXiv e-prints*, 2009, 0911.4350. Conference proceedings for Traffic and Granular Flow 2009.

[64] J. Liddle, A. Seyfried, B. Steffen, W. Klingsch, T. Rupprecht, A. Winkens, and M. Boltes. Microscopic insights into pedestrian motion through a bottleneck, resolving spatial and temporal variations. 2011, 1105.1532.

[65] A. Lindenmayer. Mathematical models for celluar interactions in development. *J. Theo. Biol.*, 18:280, 1968.

[66] X. Liu, W. Song, and J. Zhang. Extraction and quantitative analysis of microscopic evacuation characteristics based on digital image processing. *Physica A*, 388(13):2717–2726, 2009.

[67] R. Löhner. On the modelling of pedestrian motion. *Appl. Math. Model.*, 34(2):366–382, 2010.

[68] T. Meyer-König, H. Klüpfel, and M. Schreckenberg. Assessment and analysis of evacuation processes on passenger ships by microscopic simulation. In M. Schreckenberg and S. D. Scharma, editors, *Pedestrian and Evacuation Dynamics*, pages 297–302. Springer, 2002.

[69] P. Molnár. *Modellierung und Simulation der Dynamik von Fußgängerströmen.* Dissertation, Universität Stuttgart, 1995.

[70] J. Moré. The levenberg-marquardt algorithm: Implementation and theory. In G. Watson, editor, *Numerical Analysis*, volume 630 of *Lecture Notes in Mathematics*, pages 105–116. Springer, Berlin Heidelberg, 1978.

[71] M. Moussaïd, D. Helbing, S. Garnier, A. Johansson, M. Combe, and G. Theraulaz. Experimental study of the behavioural mechanisms underlying self-organization in human crowds. *Proc. R. Soc. B.*, 276(1668):2755–2762, 2009.

[72] M. Moussaïd, D. Helbing, and G. Theraulaz. How simple rules determine pedestrian behavior and crowd disasters. *P. Natl. Acad. Sci. USA.*, 108(17):6884–6888, 2011, 1105.2152.

[73] M. Moussaïd, N. Perozo, S. Harnier, D. Helbing, and G. Theraulaz. The walking behaviour of pedestrian social groups and its impact on crowd dynamics. *PLoS ONE*, 5(4):e10047, 2010.

[74] K. Müller. *Zur Gestaltung und Bemessung von Fluchtwegen für die Evakuierung von Personen aus Bauwerken auf der Grundlage von Modellversuchen.* Dissertation, Technische Hochschule Magdeburg, 1981.

[75] R. Nagai, M. Fukamachi, and T. Nagatani. Evacuation of crawlers and walkers from corridor through an exit. *Physica A*, 367:449–460, 2006.

[76] K. Nishinari, A. Kirchner, A. Namazi, and A. Schadschneider. Extended floor field CA model for evacuation dynamics. *IEICE Trans. Inf. and Syst.*, E87-D(3):726–732, 2004.

[77] K. Nishinari, K. Sugawara, and Kaza. Modelling of self-driven particles: Foraging ants and pedestrians. *Physica A*, 372(1):132–141, Dec 2006.

[78] J. Ondřej, J. Pettré, A.-H. Olivier, and S. Donikian. A synthetic-vision-based steering approach for crowd simulation. volume 29, pages 123:1 – 123:9, New York, NY, USA, 2010. ACM.

[79] D. R. Parisi and C. O. Dorso. Microscopic dynamics of pedestrian evacuation. *Physica A*, 354:606–618, 2005.

[80] D. R. Parisi and C. O. Dorso. The role of panic in the room evacuation process. *Int. J. Mod. Phys. C*, 17(3):419–434, 2006.

[81] D. R. Parisi and C. O. Dorso. Morphological and dynamical aspects of the room evacuation process. *Physica A*, 385(1):343–355, 2007.

[82] D. R. Parisi, M. Gilman, and H. Moldovan. A modification of the social force model can reproduce experimental data of pedestrian flows in normal conditions. *Physica A*, 388(17):3600–3608, 2009.

[83] W. V. Parker and J. E. Pryor. Polygons of greatest area inscribed in an ellipse. *The American Mathematical Monthly*, 51(4):205–209, 1944.

[84] J. Pauls. Suggestions on evacuation models and research questions. In T. J. Shields, editor, *Human Behaviour in Fire*, London, 2004. Intersience. Proceedings of the third International Symposium on Human Behaviour in Fire, Ulster, Belfast.

[85] N. Pelechano, K. O'Brien, B. Silverman, and N. Badler. Crowd simulation incorporating agent psychological models, roles and communication. In *First International Workshop on Crowd Simulation*, volume 2, pages 21–30, Lausanne, 2005.

[86] L. A. Pipes. An operational analysis of traffic dynamics. *J. Appl. Phys.*, 24(3):274 – 281, Mar 1953.

[87] A. Portz and A. Seyfried. Analyzing stop-and-go waves by experiment and modeling. In R. D. Peacock, E. D. Kuligowski, and J. D. Averill, editors, *Pedestrian and Evacuation Dynamics 2010*, pages 577–586, 2010.

[88] A. Portz and A. Seyfried. Modeling stop-and-go waves in pedestrian dynamics. In R. Wyrzykowski, J. Dongarra, K. Karczewski, and J. Wasniewski, editors, *PPAM 2009, Part II*, pages 561–568, Berlin Heidelberg, 2010. Springer.

[89] N. Rajewsky, L. Santen, A. Schadschneider, and M. Schreckenberg. The asymmetric exclusion process: Comparison of update procedures. *J. Stat.Phys.*, 92:151–194, 1998.

[90] A. Reuschel. Fahrzeugbewegungen in der kolonne. *Z. Öster. Ing. Arch.*, 4(193), 1950.

[91] A. Reuschel. Fahrzeugbewegungen in der kolonne bei gleichförmig beschleunigtem oder verzögertem leitfahrzeug. *Z. Öster. Ing. Arch.*, 59(73), 1950.

[92] J. Rissanen. Minimum-description-length principle. *Encyclopedia of Statistical Sciences*, 2004.

[93] A. Schadschneider. I'm a football fan ... get me out of here. *Physics World*, 21, 2010.

[94] A. Schadschneider, D. Chowdhury, and K. Nishinari. *Stochastic Transport in Complex Systems. From Molecules to Vehicles*. Elsevier Science Publishing Co Inc., 2010.

[95] A. Schadschneider, W. Klingsch, H. Klüpfel, T. Kretz, C. Rogsch, and A. Seyfried. *Encyclopedia of Complexity and System Science*, volume 5, chapter Evacuation Dynamics: Empirical Results, Modeling and Applications, pages 3142–3176. Springer, Berlin Heidelberg, 2009.

[96] A. Schadschneider and A. Seyfried. Modeling pedestrian dynamics - from experiment to theory and back. In *Traffic and Granular Flow '09*, 2009.

[97] A. Schadschneider and A. Seyfried. Validation of CA models of pedestrian dynamics with fundamental diagrams. *Cybernetics and Systems*, 40(5):367–389, 2009.

[98] K. Schindler, A. Ess, B. Leibe, and L. Van Gool. Automatic detection and tracking of pedestrians from a moving stereo rig. *ISPRS J. Photogramm.*, 65(6):523–537, 2010.

[99] V. Schneider and R. Könnecke. Simulating evacuation processes with ASERI. In M. Schreckenberg and S. D. Sharma, editors, *Pedestrian and Evacuation Dynamics 2002*, pages 303–314. Springer, 2002.

[100] M. Schreckenberg, A. Schadschneider, K. Nagel, and N. Ito. Discrete stochastic models for traffic flow. *Phys. Rev. E*, 51(4):2939–2949, 1995.

[101] A. Seyfried, M. Boltes, J. Kähler, W. Klingsch, A. Portz, T. Rupprecht, A. Schadschneider, B. Steffen, and A. Winkens. Enhanced empirical data for the fundamental diagram and the flow through bottlenecks. In W. W. F. Klingsch, C. Rogsch, A. Schadschneider, and M. Schreckenberg, editors, *Pedestrian and Evacuation Dynamics 2008*, pages 145–156, Berlin Heidelberg, 2010. Springer.

[102] A. Seyfried, O. Passon, B. Steffen, M. Boltes, T. Rupprecht, and W. Klingsch. New insights into pedestrian flow through bottlenecks. *Transport. Sci.*, 43(3):395–406, 2009.

[103] A. Seyfried, A. Portz, and A. Schadschneider. Phase coexistence in congested sates of pedestrian dynamics. In S. Bandini, S. Manzoni, H. Umeo, and G. Vizzari, editors, *Cellular Automata*, volume 6350 of *Lecture Notes in Computer Science*, pages 496–505, Berlin Heidelberg, 2010. Springer.

[104] A. Seyfried and A. Schadschneider. Empirical results for pedestrian dynamics at bottlenecks. In R. Wyrzykowski, J. Dongarra, K. Karczewski, and J. Wasniewski, editors, *Parallel Processing and Applied Mathematics*, volume 6068 of *Lecture Notes in Computer Science*, pages 575–584, Berlin Heidelberg, 2010. Springer.

[105] A. Seyfried, B. Steffen, W. Klingsch, and M. Boltes. The fundamental diagram of pedestrian movement revisited. *J. Stat. Mech.*, P10002, 2005.

[106] A. Seyfried, B. Steffen, and T. Lippert. Basics of modelling the pedestrian flow. *Physica A*, 368:232–238, 2006.

[107] W. Shao and D. Terzopoulos. Autonomous pedestrians. In K. Anjyo and P. Faloutsos, editors, *Proceedings of the 2005 ACM SIGGRAPH/Eurographics symposium on Computer animation*, SCA '05, pages 19–28, New York, NY, USA, 2005. ACM.

[108] N. Shiwakoti, M. Sarvi, G. Rose, and M. Burd. Animal dynamics based approach for modelling pedestrian crowd egress under panic conditions. *Transportation and Traffic Theory*, 17:438–461, 2011.

[109] H. Simon. Near decomposability and complexity: How a mind resides in a brain. *The Mind, The Brain, and Complex Adaptive Systems*, XXII:25–43, 1995.

[110] B. F. Skinner. *Science And Human Behavior*. Free Press, 1965.

[111] B. Steffen and A. Seyfried. The repulsive force in continous space models of pedestrian movement. *ArXiv e-prints*, 2008, 0803.1319.

[112] B. Steffen and A. Seyfried. Modelling of Pedestrian Movement around 90 and 180 Bends. In B. H. V. Topping and Y. Tsompanakis, editors, *Proceedings of the First International Conference on Soft Computing Technology in Civil, Structural and Environmental Engineering*. Civil-Comp Press, Stirlingshire, UK, 2009,, 2009.

[113] B. Steffen and A. Seyfried. Methods for measuring pedestrian density, flow, speed and direction with minimal scatter. *Physica A*, 389(9):1902–1910, 2010.

[114] A. Steiner, M. Philipp, and A. Schmid. Parameter estimation for a pedestrian simulation model. In *Swiss Transport Research Conference*, 2007.

[115] Y. Suma, D. Yanagisawa, and K. Nishinari. Anticipation effect in pedestrian dynamics: Modelling and experiments. *Physica A*, 391:248–263, 2012.

[116] J. A. Templer. *The Staircase: Studies of Hazards, Falls, and Safer Design*. The MIT Press, Massachusetts, 1992.

[117] P. A. Thompson and E. W. Marchant. A computer model for the evacuation of large building populations. *Fire Safety J.*, 24:131–148, 1995.

[118] P. A. Thompson and E. W. Marchant. Testing and application of the computer model 'SIMULEX'. *Fire Safety J.*, 24:149–166, 1995.

[119] J. van den Berg, M. Lin, and D. Manocha. Reciprocal velocity obstacles for real-time multi-agent navigation. In *Robotics and Automation, 2008. ICRA 2008. IEEE International Conference on*, pages 1928–1935, 2008.

[120] P. Viola, M. J. Jones, and D. Snow. Detecting pedestrians using patterns of motion and appearance. In *IEEE International Conference on Computer Vision*, volume 2, pages 734–741, 2003.

[121] U. Weidmann. Transporttechnik der Fussgänger. Technical Report Schriftenreihe des IVT Nr. 90, Institut für Verkehrsplanung,Transporttechnik, Strassen- und Eisenbahnbau, ETH Zürich, ETH Zürich, 1993. Zweite, ergänzte Auflage.

[122] T. Werner and D. Helbing. The social force pedestrian model applied to real life scenarios. In E. R. Galea, editor, *Pedestrian and Evacuation Dynamics 2003*, pages 17–26, London, 2003. CMS Press.

[123] S. Wolfram. Statistical mechanics of cellular automata. *Rev. Mod. Phys.*, 55:601–644, 1983.

[124] K. Yamamoto, S. Kokubo, and K. Nishinari. Simulation for pedestrian dynamics by real-coded cellular automata (RCA). *Physica A*, 379:654–660, 2007.

[125] K. Yamori. Going with the flow: Micro-macro Dynamics in the macrobehavioral patterns of pedestrian crowds. *Psycholog. Rev.*, 105(3):530–557, 1998.

[126] D. Yanagisawa, A. Kimura, A. Tomoeda, N. Ryosuke, Y. Suma, K. Ohtsuka, and K. Nishinari. Introduction of frictional and turning function for pedestrian outflow with an obstacle. *Phys. Rev. E*, 80(3):036110, 2009.

[127] D. Yanagisawa and K. Nishinari. Mean-field theory for pedestrian outflow through an exit. *Phys. Rev. E*, 76:061117, 2007.

[128] D. Yanagisawa, A. Tomoeda, and K. Nishinari. Improvement of pedestrian flow by slow rhythm. *Physical Review E*, 85(1):016111, 2012.

[129] W. Yu and A. Johansson. Modeling crowd turbulence by many-particle simulations. *Phys. Rev. E*, 76:046105, 2007.

[130] W. J. Yu, L. Chen, R. Dong, and S. Dai. Centrifugal force model for pedestrian dynamics. *Phys. Rev. E*, 72(2):026112, 2005.

[131] J. Zhang, W. Klingsch, A. Schadschneider, and A. Seyfried. Transitions in pedestrian fundamental diagrams of straight corridors and t-junctions. *J. Stat. Mech.*, 2011.

[132] J. Zhang, W. Klingsch, A. Schadschneider, and A. Seyfried. Ordering in bidirectional pedestrian flows and its influence on the fundamental diagram. *J. Stat. Mech.*, (2), 2012.

[133] J. Zhang, W. Klingsch, and A. Seyfried. High precision analysis of unidirectional pedestrian flow within the Hermes project. In *The Fifth Performance-based Fire Protection and Fire Protection Engineering Seminars*, 2010.

[134] X. Zheng and P. Palffy-Muhoray. Distance of closest approach of two arbitrary hard ellipses in two dimensions. *Phys. Rev. E*, 75(6):061709, 2007.

APPENDIX E

Erklärung

Ich versichere, dass ich die von mir vorgelegte Dissertation selbständig angefertigt, die benutzten Quellen und Hilfsmittel vollständig angegeben und die Stellen der Arbeit – einschließlich Tabellen, Karten und Abbildungen –, die anderen Werken im Wortlaut oder dem Sinn nach entnommen sind, in jedem Einzelfall als Entlehnung kenntlich gemacht habe; dass diese Dissertation noch keiner anderen Fakultät oder Universität zur Prüfung vorgelegen hat; dass sie – abgesehen von unten angegebenen Teilpublikationen – noch nicht veröffentlicht worden ist sowie, dass ich eine solche Veröffentlichung vor Abschluss des Promotionsverfahrens nicht vornehmen werde. Die Bestimmungen der Promotionsordnung sind mir bekannt. Die von mir vorgelegte Dissertation ist von Prof. Dr. Andreas Schadschneider betreut worden.

Mohcine Chraibi, den 15. März 2012